Journal Pre-proofs

Research paper

The mixing method used to formulate lipid nanoparticles affects mRNA delivery efficacy and organ tropism

Daria M. Strelkova Petersen, Namit Chaudhary, Mariah L. Arral, Ryan M. Weiss, Kathryn A. Whitehead

PII: S0939-6411(23)00266-7
DOI: https://doi.org/10.1016/j.ejpb.2023.10.006
Reference: EJPB 14118

To appear in: *European Journal of Pharmaceutics and Biopharmaceutics*

Received Date: 29 January 2023
Revised Date: 30 September 2023
Accepted Date: 4 October 2023

Please cite this article as: D.M. Strelkova Petersen, N. Chaudhary, M.L. Arral, R.M. Weiss, K.A. Whitehead, The mixing method used to formulate lipid nanoparticles affects mRNA delivery efficacy and organ tropism, *European Journal of Pharmaceutics and Biopharmaceutics* (2023), doi: https://doi.org/10.1016/j.ejpb.2023.10.006

The mixing method used to formulate lipid nanoparticles affects mRNA delivery efficacy and organ tropism

Daria M. Strelkova Petersen[1], Namit Chaudhary[2], Mariah L. Arral[2], Ryan M. Weiss[2], Kathryn A. Whitehead[1,2,*]

[1]Department of Biomedical Engineering, Carnegie Mellon University, 5000 Forbes Ave, Pittsburgh, PA, 15213

[2]Department of Chemical Engineering, Carnegie Mellon University, 5000 Forbes Ave, Pittsburgh, PA, 15213

*Corresponding Author: Kathryn A. Whitehead, kawhite@cmu.edu

Abstract

mRNA is a versatile drug molecule with therapeutic applications ranging from protein replacement therapies to in vivo gene engineering. mRNA delivery is often accomplished using lipid nanoparticles, which are formulated via mixing of aqueous and organic solutions. Although this has historically been accomplished by manual mixing for bench scale science, microfluidic mixing is required for scalable continuous manufacturing and batch to batch control. Currently, there is limited understanding on how the mixing process affects mRNA delivery efficacy, particularly in regard to tropism. To address this knowledge gap, we examined the influence of the type of mixing and microfluidic mixing parameters on the performance of lipid nanoparticles in mice. This was accomplished with a Design of Experiment approach using four nanoparticle formulations with varied ionizable lipid chemistry. We found that each formulation required unique optimization of mixing parameters, with the total delivery efficacy of each lipid nanoparticle generated with microfluidics ranging from 100-fold less to 4-fold more than manually mixed LNPs. Further, mixing parameters influenced organ tropism, with the most efficacious formulations disproportionately increasing liver delivery compared to other organs. These data suggest that mixing parameters for lipid nanoparticle production may require optimization for each unique chemical formulation, complicating translational efforts. Further, microfluidic parameters must be chosen carefully to balance overall mRNA delivery efficacy with application-specific tropism requirements.

Keywords: lipid nanoparticles; LNPs; mRNA delivery; RNA delivery; IVIS imaging; ionizable lipids; microfluidics mixing; Benchtop NanoAssemblr

1. Introduction

In recent years, lipid nanoparticles (LNPs) have graduated from a niche technology to a clinically proven tool that has been successfully deployed in hundreds of millions of people worldwide via the COVID-19 mRNA vaccines [1,2]. Beyond vaccines, mRNA LNPs are being developed for a broad range of applications, including zinc finger and CRISPR-based gene editing systems [3–9], protein replacement therapy [10–15], and cancer treatments [16–23]. Since naked mRNA is quickly degraded by nucleases in the blood and extracellular compartments [24,25], mRNA requires a vehicle that protects and delivers it into the cytoplasm of target cells. Out of all viral and non-viral RNA delivery vehicles, LNPs are the most clinically advanced and carry the lowest risks of inflammation or other adverse events [23]. In addition to the approved vaccines, numerous LNP-based mRNA therapeutics are in clinical trials, including for the treatment of glycogen storage disease type 1a [26,27], ornithine transcarbamylase deficiency [28], and transthyretin amyloidosis [29].

LNPs are complex, multi-component delivery vehicles in which mRNA is encapsulated by a combination of synthetic and natural lipids [30]. These lipids typically include an ionizable cationic lipid or lipidoid, a “helper” lipid (often a phospholipid), cholesterol, and a lipid conjugated to polyethylene glycol (PEG-lipid) [31]. They are generated by mixing an aqueous buffer containing mRNA with an ethanol solution containing lipid components. Upon mixing, electrostatic and hydrophobic/hydrophilic interactions drive the coalescence of nanoparticles, a process sometimes referred to as nanoprecipitation [32]. Resultant particles can range widely in size, with the final size determined by lipid chemistry, the percentage of PEG in the formulation, and the mixing conditions [33,34].

The mixing of the aqueous and organic streams is an important part of this process and, over the years, has been accomplished in two primary ways: manual and microfluidic mixing. Manual mixing is generally used for small, bench scale volumes (100 µl to 4 ml) and is accomplished using standard pipets and a vortex [35]. Alternatively, microfluidic mixing involves specialized equipment that mixes large volumes of LNPs in a continuous process, which enables consistent large-scale manufacturing. Many early studies that delivered RNA with lipid nanoparticles used manual mixing techniques [24,36–39]. Currently, some labs continue to mix their LNPs manually, while others use in-house [40,41] or commercially designed [42]

microfluidic devices. There are several possible architectural designs of the mixing channel that combine the mRNA and lipid streams, including T-mixing, Y-mixing and ring mixing [43].

Although, historically, bench scale formulations have been generated manually [44], there is limited information on the effect of scale-up using microfluidics on the in vivo performance of these formulations. Ideally, LNPs generated via microfluidics will behave identically to those made manually, including both overall efficacy and organ distribution. It's unclear that this would be the case, given that pipette mixing controls neither the exact flow rate of the two solutions nor the architecture of mixing, whereas these parameters are automated with microfluidics. Studies with microfluidic devices use a wide range of flow rates (4-14 ml/min) with little discussion on rationale for those choices [43,45–52]. Further, the 1:1 volumetric ratio of aqueous to ethanol solutions used for manual mixing is often changed to 2:1 or 3:1 when using microfluidics [40,48,51,52]. Indeed, the ability to vary the total flow rate and volumetric stream ratios results in a large design space by which to create LNPs using microfluidic devices.

The goal of this study was to improve understanding of how manual and microfluidic formulations compare in terms of in vivo performance in terms of both efficacy and tropism. Although efficacy is frequently discussed in the literature, limited attention has been paid to the challenges of tropism changes that can occur during scale-up. Although most LNPs target the liver [23,53,54], there is an increasing number of studies that describe extrahepatocellular delivery. [23,54–56]. As each of these formulations are developed for cell- and organ- specific applications, it is important to understand how mixing parameters affect scale-up with microfluidic devices as to retain the intended utility.

To accomplish this, we worked with two LNPs, each with a distinct ionizable lipid. In addition to formulating these manually, we generated microfluidic formulations on a commercially available microfluidics mixer (Benchtop™ Precision Nanosystems) employing a Y-mixing herringbone architecture [57]. We evaluated a library of mixing parameters generated by Design of Experiment and tested resultant LNP physical properties and in vivo behavior (total efficacy and organ tropism). Results indicate that each LNP requires optimization of mixing parameters. Further, the mixing parameters that yielded LNPs with improved in vivo efficacy did so by increasing liver delivery, which may or may not be beneficial depending on the treatment application. Together, these data provide evidence that microfluidic parameters should be

optimized for each LNP, and that performance can vary across manual and microfluidic formulations.

2. Materials and Methods

2.1 Materials

Amine 3,3′-diamino-*N*-methyldipropylamine (306) and isodecyl acrylate (O_{i10}) and undecyl acrylate (O_{10}) were sourced from Sigma-Aldrich (St Louis, MO). Amines N1,N1'-(propane-1,3-diyl)bis(N1-methylethane-1,2-diamine) (503) and N1,N1'-(propane-1,3-diyl)bis(N1-ethylethane-1,2-diamine) (514) were synthesized in the lab (see SI Methods section). 2-Hexyl-Decyl Acrylate ($O_{6,10}$) was also made in the lab (see SI Methods section). 1,2-dioleoyl-*sn*-glycero-3-phosphoethanolamine (DOPE) and 14:0 PEG2000 PE (PEG 2000) was purchased from Avanti Polar Lipids (Alabaster, AL). Cholesterol was sourced from Sigma-Aldrich (St Louis, MO). Luciferase mRNA was purchased from Trilink Biotechnologies (San Diego, CA). Monobasic citrate and 2-(p-toluidinyl)naphthalene-6-sulphonic acid (TNS) were sourced from Sigma-Aldrich (St Louis, MO). 3.5 MWCO Dialysis Cassettes and Quanti-iT RiboGreen were purchased from Thermo Fisher Scientific (Waltham, MA). Phosphate buffer saline at pH 7.4 was sourced from VWR (Randor, PA). Black 96 well flat bottom plates were purchased from GreineerBio through VWR (Randor, PA). D-Luciferin was sourced from PerkinElmer (Waltham, MA).

2.2 Lipidoid Synthesis

Ionizable lipidoids were synthesized by combining alkyl-amines with alkyl-acrylate tails at a stoichiometric ratio of 1:4 in a scintillation vial and stirring at 90 °C for 3 days [1]. Amines 3,3′-diamino-*N*-methyldipropylamine (306) and N1,N1'-(propane-1,3-diyl)bis(N1-methylethane-1,2-diamine) (503) were reacted with isodecyl acrylate (O_{i10}) to form the $306O_{i10}$ and $503O_{i10}$ lipidoids, respectively. Amine N1,N1'-(propane-1,3-diyl)bis(N1-ethylethane-1,2-diamine) (514) was reacted with acrylate $O_{6,10}$ to form $514O_{6,10}$ lipidoid, and amine 3,3′-diamino-*N*-methyldipropylamine (306) was reacted with undecyl acrylate (O_{10}) to form $306O_{10}$ lipidoid. Synthesized lipidoids were purified with Teledyne ISCO Chromatography system (Thousand Oaks, CA) and resulting fractions were verified with mass spectroscopy to contain $306O_{i10}$ and $503O_{i10}$, $306O_{10}$, and $514O_{6,10}$ lipidoids respectively.

2.3 Lipid Nanoparticle Fabrication

Lipid nanoparticles (LNPs) were formulated in one of two ways by mixing a lipid solution with an aqueous mRNA solution, as previously described [53]. The lipid solution contained ionizable lipidoid, cholesterol, DOPE, and PEG2000. These four compounds were dissolved in 90% ethanol and 10% pH 4 citrate buffer by volume at a molar ratio of 35:46.5:16:2.5. An aqueous solution was made containing 5-methoxyuridine (5moU) base-modified firefly luciferase-encoding mRNA (mLuc), dissolved in 10 mM citrate buffer (pH 4) so that the resulting lipidoid to mRNA ratio was 10:1 (w/w). LNPs were made at 0.05 mg/ml mRNA concentration.

LNPs were formulated either manually or using microfluidics. For LNPs formulated manually, a pipette was used to add lipid solution to the mRNA solution at a volumetric ratio of 1:1. Immediately after addition, the resulting solution was vortexed on maximum speed (3200 rpm) for 5 s. For LNPs formulated using microfluidics, the Nanoassemblr™ Benchtop (Precision Nanosystems, Vancouver, Canada) was used. Lipid and mRNA solutions were added to respective input microfluidics channels. Flow rate (4, 8, 11, 10, 12 or 14 ml/min) and volumetric ratio of mRNA solution to lipid solution (1:1, 3:2, 2:1, 3:1) was varied for each formulation. After mixing all LNPs were diluted 1:1 with PBS to achieve desired mRNA concentration and decrease ethanol percentage in the mixture.

All LNPs were then dialyzed against phosphate buffered saline (PBS, VWR, Randor, PA) in a dialysis cassette (Thermo Fisher, Waltham, MA) with a 3.5 kDa molecular weight cut off membrane for 1 hour.

2.4 Lipid Nanoparticles Characterization

Each batch of LNPs was characterized prior to use in animal experiments. LNPs were diluted with PBS to 0.005 mg/ml mRNA concentration. This solution was used to measure nanoparticle size using dynamic light scattering (Malvern Zetasizer Nano ZSP, Malvern, UK). Both zeta average diameter and number average diameter were measured. Separately, RNA entrapment was determined using the Quant-iT RiboGreen assay according to manufacturer's instructions and in accordance with our previous publications [58]. Briefly, LNPs were diluted with PBS to 0.005 mg/ml mRNA concentration, mixed 1:1 with 1x TE buffer or 1% TritonX buffer, and incubated with the RiboGreen reagent for 15 min at 37^{o}C. Resulting fluorescence was quantified by plate reader (Ex 480 nm/ Em 525 nm).

2.4.1 TNS ionization

2-(p-toluidinyl)naphthalene-6-sulphonic acid (TNS) fluorescent probe was used to measure LNP ionization at pH 5.0, as previously described [59]. 250 µl of TNS buffer (150 mM sodium chloride, 20 mM sodium phosphate, 20 mM ammonium acetate and 25 mM ammonium citrate; pH adjusted to 5.0 after mixing) was added per well to a black 96 well plate. Then 5 µl of LNP (0.05 mg/ml mRNA concentration) and 10 µl of 0.16 mM TNS stock solution was added. Resulting fluorescence signal was measured immediately using Synergy H1 plate reader (BioTek). Fluorescent signal corresponded to positive ionization.

2.5 Animal Experiments

All animal experiments were conducted using institutionally approved protocols (IACUC) and in accordance with state and local regulations. We used a Firefly luciferase – D-Luciferin reporter system to assess LNP efficacy in mice. LNPs were formulated with luciferase mRNA at a total mRNA dose of 0.05 mg/ml. A minimum of three animals were used per each group, and naked mRNA was used as negative control. LNPs were injected via tail vein into 6-8 week old C57BL/6 female mice (Charles River Laboratories, Wilmington, MA) at a total mRNA dose of 0.5 mg/kg. Three hours after LNP injection, 130 µl of 30 mg/ml D-luciferin was injected intraperitonealy. Fifteen minutes later, mice were sacrificed using CO_2 gas and cervical dislocation. Liver, spleen, lungs, heart, pancreas, and kidneys were transferred to black paper. Luminescence signal was measured three hours and fifteen minutes after LNP injection using an in vivo imaging system (IVIS, PerkinElmer, Waltham, MA).

2.6 Design of Experiments

The DOE library was generated using Design Expert software (Stat-Ease, Minneapolis, MN). Lipidoid ($306O_{i10}$ or $503O_{i10}$), flow rate (4-14 ml/min) and aqueous to lipidoid ratio (1:1, 3:2, 2:1, 3:1) were used as input parameters. D-optimal design model for a randomized response surface analysis was used to generate the library in Table 1. Then that library was expanded by testing each lipidoid with each mixing parameter combination.

2.7 Statistics

All graphs and statistical data were generated using GraphPad Prism software (GraphPad, San Diego, CA) version 7.0.

3. Results

This study compares the efficacy and organ distribution of lipid nanoparticle (LNP) formulations made by hand and with a microfluidic device. LNPs for bench scale work are often generated using a straightforward pipette mixing technique, given its ease and the ability to tailor volumes to the exact experimental needs, which in turn conserves costly RNA [45,46]. However, microfluidic devices are required for scale-up and clinical translation because their controlled mixing parameters facilitate reproducibility and continuous process manufacturing [43]. In response to the increased interest in LNPs and nucleic acid delivery over the last decade, some labs have developed fabrication techniques to create microfluidic devices in-house; bench scale mixers have also become commercially available [45,46,60,61].

Although manual mixing protocols are well-established [59,62], microfluidic systems introduce several mixing parameters that require selection. Although this selection is aided by previous studies [63,64], there is little information on the preservation of LNP in vivo potency and tropism during scale-up using microfluidic systems. In this work, we sought to fill this knowledge gap by determining the best mixing parameters that maintain LNP potency and organ specificity when using a microfluidics device.

To accomplish this, we analyzed a small set of mixing parameters to identify the best parameters for formulating LNPs containing two different ionizable lipids. In addition to the selection of solution concentrations as with hand mixing, microfluidic mixing introduces two more variables: 1) the volumetric ratio of the mRNA aqueous solution to the lipid ethanol solution, and 2) the overall flow rate of the system.

3.1 Microfluidic mixing parameters were optimized for two LNPs

Our goal was to identify optimal mixing parameters for two LNPs containing the unique ionizable lipidoids, $306O_{i10}$ [53] and $503O_{i10}$. We will refer to LNPs generated from these lipidoids as LNP 1 and LNP 2, respectively. In these experiments, the LNPs were formulated either by hand or using microfluidics with the following ingredients: ionizable lipidoid, cholesterol, the helper lipid DOPE, C_{14}-PEG lipid, and mRNA encoding firefly luciferase (mLuc). The first four ingredients were diluted in ethanol, and mRNA was diluted in citrate buffer to make an aqueous solution. To create LNPs, ethanol and aqueous solutions were mixed by hand or via

a chaotic herringbone microfluidics mixing chip. Mice were IV-injected with resulting LNPs at a total mLuc dose of 0.5 mg/kg, and resultant luciferase expression was quantified 3 hours post-injection.

When formulated by hand, LNP 1 (Figure 1A and 1C) was the most potent, consistent with previous studies from our group [53,65]. Here, it produced 10^9 p/s total luciferase signal in vivo with up to 97% of the signal in the liver. LNP 2 (Figure 1B and 1D) has not been previously described; it was chosen for this study because of its efficacy and its spleen and lung targeting potential. LNP 2 was synthesized in the lab and confirmed by mass spectroscopy (SI Methods and SI Figure 1). In this study, its total luciferase signal in vivo was 10^8 p/s, with 30% and 2% of the signal coming from the spleen and lungs, respectively. The ionizable lipidoids in LNPs 1 and 2 have similar molecular weights, head structures, and number of hydrophobic tails (Figure 1C and D). In all in vivo experiments performed in this study, negative control groups included untreated animals and those injected with naked mRNA. These groups produce background luminescent signal on the order of 10^5 p/s and are not shown here.

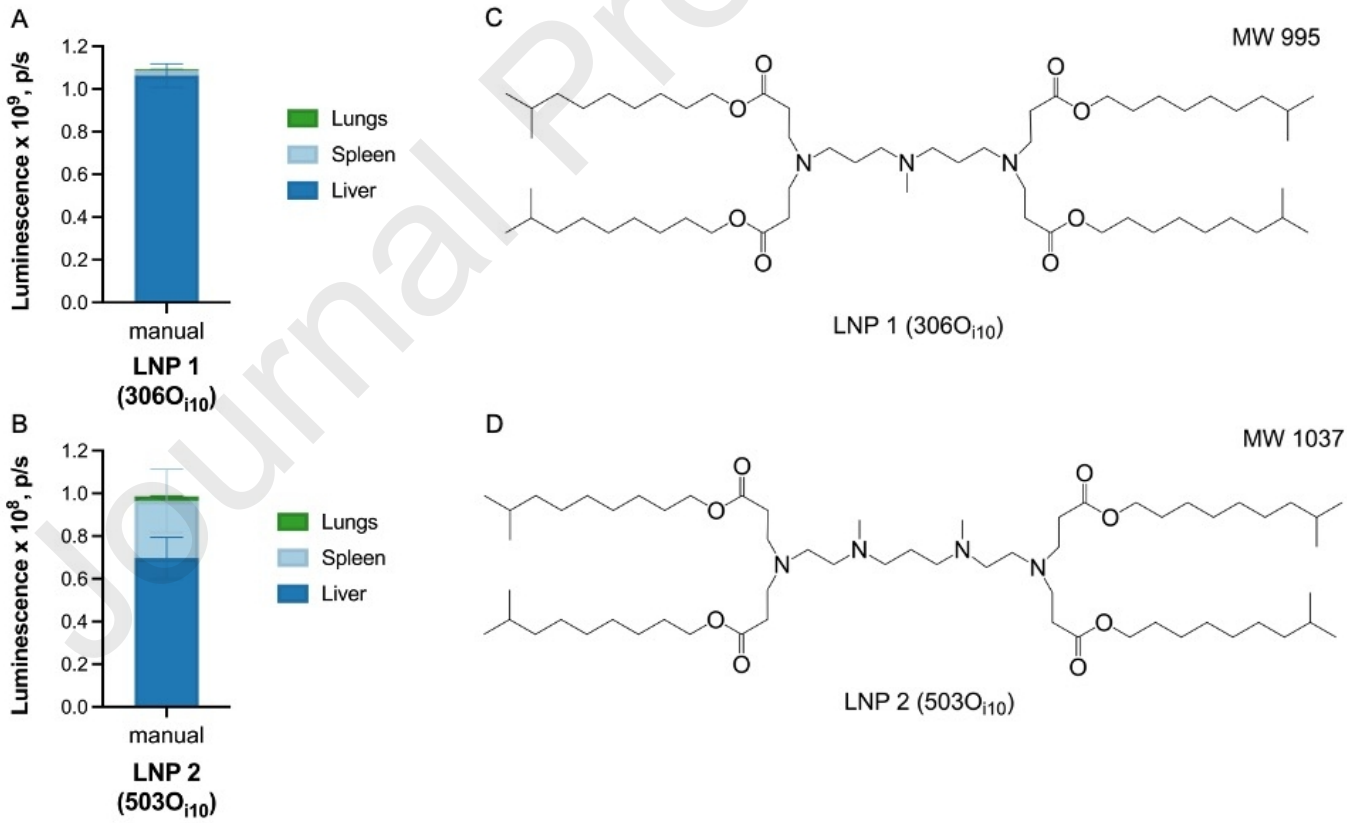

Figure 1. Lipid nanoparticles 306O$_{i10}$ (LNP 1) and 503O$_{i10}$ (LNP 2) are structurally similar but have different organ tropism. *LNP 1 (A) and LNP 2 (B) were manually formulated with*

mLuc and IV-injected at a total mRNA dose of 0.5 mg/kg. Three hours later, luminescent signal in the liver, spleen, and lungs was measured via IVIS. N = 3, error bars represent standard deviation. (C, D) Ionizable lipid structures with corresponding molecular weight in g/mol.

To select optimal mixing parameters, we first looked at what parameter combinations have been successful in the literature [66,67]. We used these literature values to create a design of experiment (DoE) based library of mixing parameters (Table 1). We have measured total and by-organ efficiency of the resulting LNPs in vivo as well as LNP size, mRNA entrapment and surface ionization values at pH 5. The five best-performing parameter combinations were tested with an additional two LNPs made with unique ionizable lipidoids (SI Figure 2) to see if there were similarities among mixing conditions that produce efficient LNPs. We wanted to know if mixing parameters are universal between different LNPs and looked for relationships between solution ratios, mixing speeds, and in vivo efficacy.

Mixing condition	Flow Rate, ml/min	Aqueous to Ethanol solutions ratio (v:v)
A	4	1.5:1
B	11	3:1
C	14	1:1
D	4	3:1
E	4	1:1
F	14	2:1
G	14	3:1
H	8	1:1
I	12	1:1
J	10	2:1

Table 1. ***DoE based microfluidics mixing parameters used for each of the mixing conditions****. Mixing conditions were generated by Design of Experiment software for the most efficient coverage of the parameter space. Flow rate (4-14 ml/min), volumetric aqueous to ethanol solutions ratio (1:1, 2:1, 3:1 and 3:2 ratios), and ionizable lipid were used as input parameters. The generated library was then expanded to test each condition with both lipids, resulting in 10 mixing conditions.*

3.1 Mixing parameters did not perform uniformly for LNP 1 and 2

First, we compared the efficacy and organ distribution for LNPs generated using manual mixing procedures to those using microfluidics. All microfluidic LNPs in this study were generated with a Benchtop NanoAssemblr™ from Precision Nanosystems according to the 10 mixing conditions (A – J) described in Table 1. LNPs were then IV-injected into C57BL/6 mice at a total mLuc dose of 0.5 mg/kg, and bioluminescence signal was quantified in five major murine organs three hours after injection. Resulting total luminescence signal is shown in Figure 2.

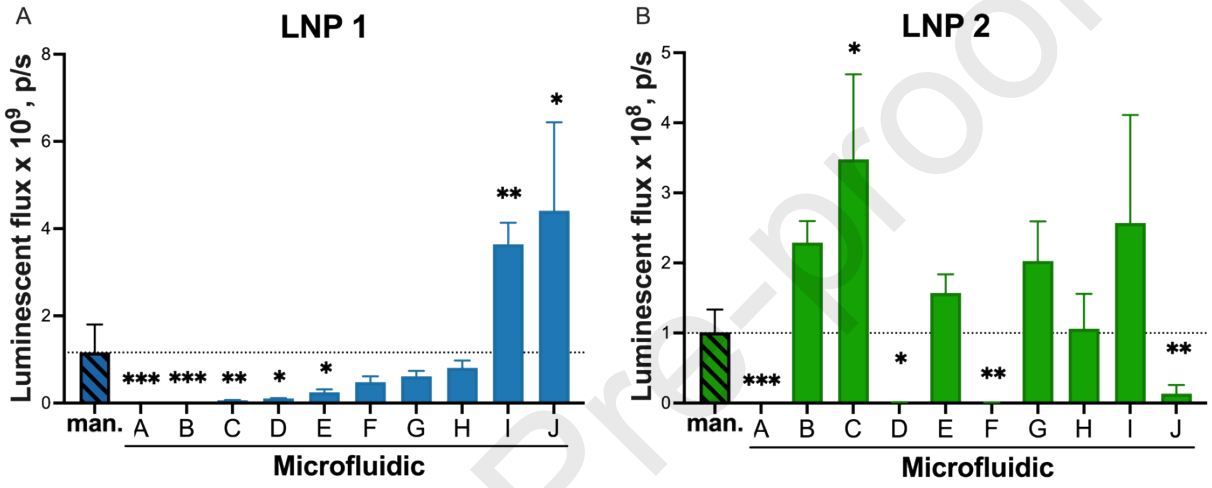

Figure 2. ***The mixing conditions used to formulate lipid nanoparticles impacted mRNA delivery efficacy.*** *Design of Experiments identified 10 sets of microfluidic mixing conditions A-J for LNP formulation and testing (see Table 1 for mixing conditions). The mixing variables included flow rate and the volumetric ratio of aqueous to ethanol streams. These nanoparticles were formulated with one of two LNPs: A) LNP 1 or B) LNP 2. Mice were dosed with 0.5 mg/kg total mRNA encoding firefly luciferase. Efficacy was quantified by luminescent flux via IVIS imaging and manually mixed nanoparticles are shown with striped bars. N = 3, error bars represent s.d., with *, **, *** representing p<0.05, 0.01, 0.005, respectively, according to a parametric two-tailed t-test.*

Depending on the mixing parameters, LNPs performed from 100x worse to 4x better than LNPs made manually. For LNP 1, only two microfluidic formulations (I and J) improved potency, up to 4x, compared to the manual formulation (Figure 2A). For LNP 2, five formulations (B, E, G, H, I) produced comparable efficacy to the manual formulation, and one formulation, C, improved efficacy 2-fold (Figure 2B). Although the most potent formulations experienced more variability in efficacy quantification, several nonetheless outperformed manually mixed formulations with statistical significance.

Interestingly, mixing parameters did not perform uniformly across formulations. For example, microfluidic mixing conditions B and C performed well for LNP 2 and poorly for LNP 1,

while the reverse is true for mixing condition J. This suggests that mixing parameters may require experimental optimization for each LNP of interest.

3.2 Mixing parameters increase signal distribution to the spleen and liver in the most efficient LNP formulations

In addition to efficacy, we examined whether the distribution of luciferase signal as a function of organ changes when microfluidic mixing parameters are altered. This is an important consideration, given that therapeutic applications are reliant on precise delivery to relevant organs. For example, to treat cystic fibrosis, LNP cargo would be delivered ideally only to lung tissue. Systemic CAR-T therapy, on the other hand, would require mRNA delivery to T-cells throughout the body. Therefore, when an LNP formulation is developed for these applications, it is vital that in vivo signal distribution is retained between LNPs mixed manually and LNPs mixed using a microfluidics chip.

We next examined whether signal distribution as a function of organ would remain the same for LNPs generated via microfluidic mixing versus manually. Figure 3 shows the bioluminescence signal distribution for LNPs from Figure 1 that performed >25% of the manually mixed LNPs. LNP 1 has a typical organ signal distribution, with most of its signal in the liver [53]. Specifically, 97, 2, and 0.3% of its luminescent expression originated from the liver, spleen, and lungs, respectively. For LNP 1 generated by microfluidic mixing (Figure 3A), the liver remained as the source of 94% of the signal. The best performing mixing condition for LNP 1 (J), however, produced a significantly higher fraction of the signal in the spleen (up to 6% vs. 2%, Figure 3A). This higher spleen signal percentage is due to increased efficacy in the spleen (SI Figure 3), as opposed to lower overall efficacy.

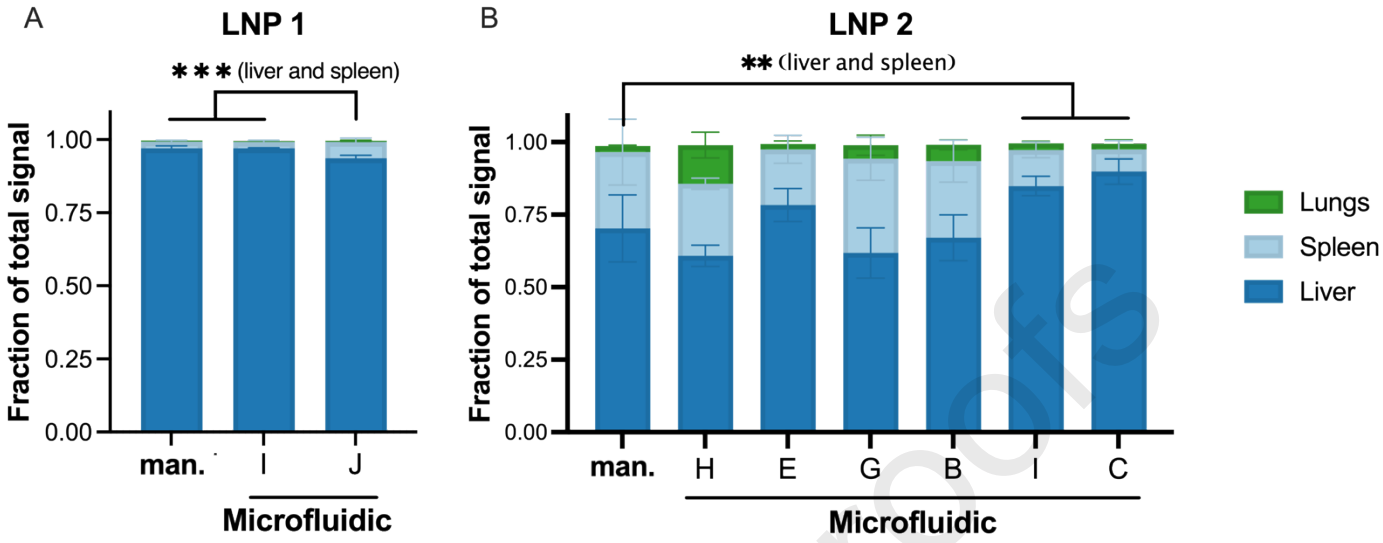

Figure 3. The mixing conditions used to formulate mRNA-loaded LNPs can shift LNP tropism. *LNPs generated via microfluidic mixing with >25% of the manual (man.) LNP efficacy are shown here. LNPs were formulated with mRNA encoding firefly luciferase and delivered to mice at a total mRNA dose of 0.5 mg/kg. A) LNP 1 is highly liver-tropic, regardless of formulation conditions. B) LNP 2 is spleen- and lung-tropic when mixed manually and liver-tropic when mixed using I and C microfluidic mixing conditions. N=3, error bars represent standard deviation, *** indicates p<0.001 according to a Dunnett multiple comparison analysis after two-way ANOVA.*

LNP 2 transfects spleen to a higher degree than LNP 1, with a signal distribution of 68% liver, 30% spleen and 2% lung. For LNP 2, when mixed using microfluidics, there were nonsignificant differences in lung signal percentage. The best performing mixing conditions (I and C) significantly decreased spleen signal percentage and increased liver signal percentage. It is possible that this change in organ distribution is due to an increase in total signal in the liver of I and C mixing conditions (SI Figure 3). Further research is needed to determine why and how certain mixing parameters can cause increased signal in the liver or spleen. Also, LNPs with tropism to extrahepatocellular organs, like LNP 2, need to be tested for organ distribution when made via microfluidics mixing to ensure retention of their unique features.

3.3 *Each new LNP required optimization of mixing parameters*

Next, we asked how mixing condition performance extended to additional LNP chemistries. For these studies, we tested two more LNPs containing unique ionizable lipidoids, each using the five mixing conditions from Table 1 (C, B, H, I, and J) that improved upon the manual formulation performance of the LNPs 1 and 2. We wondered if LNPs 1 and 2 were too

different in total efficacy or signal distribution to perform optimally under the same mixing conditions. Therefore, the two additional LNPs (LNPs 3 and 4) that we selected had similar organ tropism to LNPs 1 and 2 when formulated manually. The ionizable lipidoid in LNP 3, $306O_{10}$, is structurally similar to LNP 1 with the only difference being the isomeric tail (SI Figure 2). When made by hand and IV-administered at a total mLuc dose of 0.5 mg/kg, LNP 3 produced up to 95% of its bioluminescent signal in the liver and increased to $3*10^8$ p/s total signal (Figures 4A and 4C). LNP 4 exhibited similar total signal and organ tropism to LNP 2 (60% liver, 25% spleen, 15% lungs) (Figures 4B and 4D).

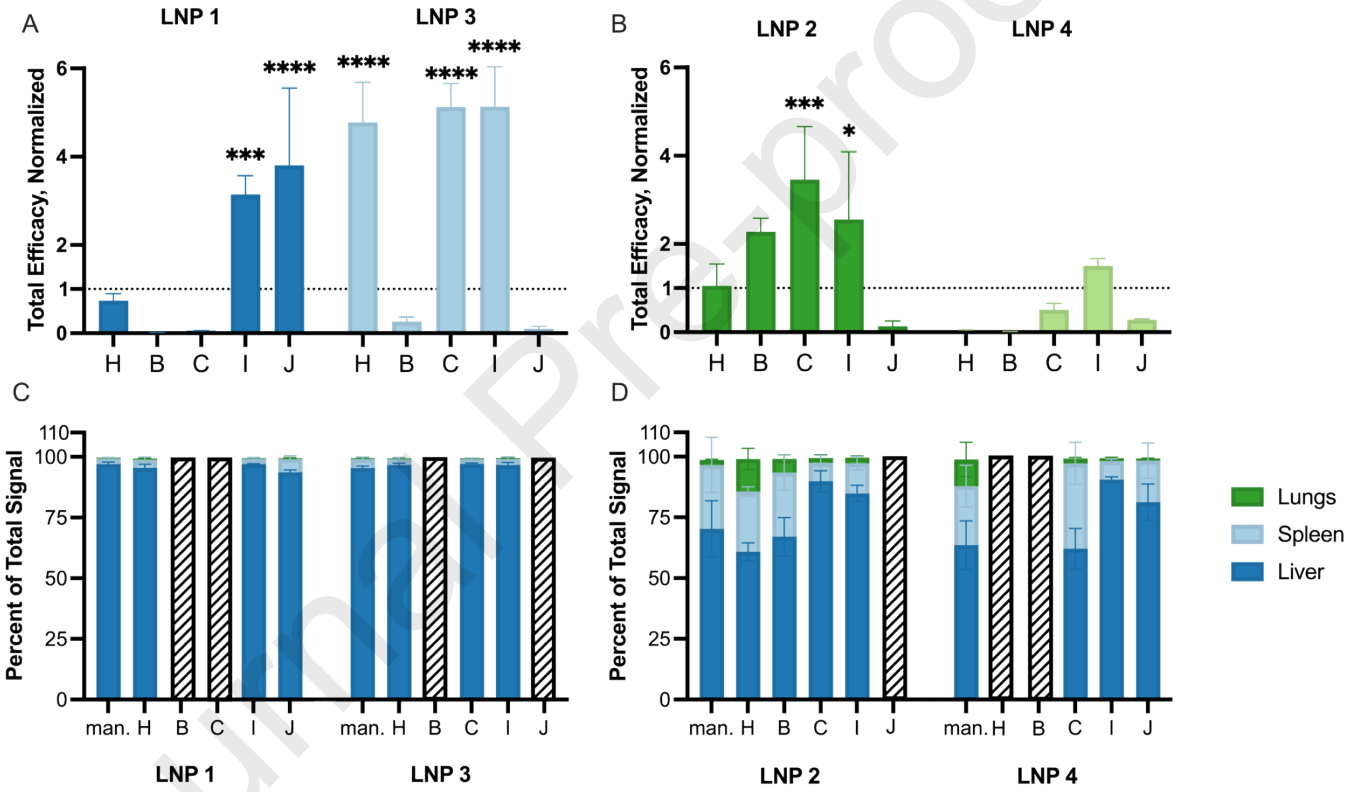

Figure 4. ***Mixing conditions must be optimized for each LNP.*** *LNPs 1-4 were generated using five sets of mixing conditions. Mice were IV-injected with mRNA encoding firefly luciferase at a total dose of 0.5 mg/kg. Panels A) and B) show total efficacy for each LNP, normalized to that of the manually mixed LNP. The most efficacious mixing conditions were not consistent across the LNPs. Panels C) and D) show the efficacy distribution between liver, spleen and lungs for formulations mixed manually (man.) and using microfluidics. Striped bars indicate that the formulation was insufficiently efficacious to examine tropism. N=3, error bars represent standard deviation. *, ***, **** represent p<0.05, 0.005 and 0.001, respectively, compared to the efficacy of manually formulated LNPs according to a parametric two-tailed t-test.*

Unfortunately, we again saw that there are no mixing parameters that would yield high total signal across all LNPs (Figures 4A and 4B). Although the mixing parameter combination I worked at least as well as the manual formulation for all four LNPs, further studies are needed to determine if its potency extends to additional LNP formulations. LNP 3 signal percentage by organ didn't change when mixed via microfluidics (Figure 4C). Meanwhile, as with LNP 2, the liver signal percentage increased with the potent LNP 4 (Figure 4D, formulation I). This trend can be explained by an increase in total liver signal in LNPs 3 and 4 (SI Figure 4).

3.4 *Microfluidic mixing parameters did not correlate well with LNPs in vivo efficacy or their physical characteristics*

Next, we examined possible correlations between mixing parameters, LNP in vivo efficacy, and LNP physical parameters like entrapment and particle size. For all manual and microfluidic formulations of LNPs 1 and 2, we measured Z-average and number mean size using dynamic light scattering and mRNA entrapment using the RiboGreen™ assay. Surface charge was also measured via the TNS assay at pH 5, which determines LNP ionization levels as a function of pH [36,68,69]. We measured surface charge at pH 5 because we previously found that that this parameter correlated with in vivo efficacy [59].

These characterization data were input into Design Expert DoE software to produce a correlation matrix for mixing conditions, LNP efficacy, and physical parameters (Figure 5A). Mixing ratio has the strongest correlations with LNP characteristics: positive correlation with entrapment % and TNS ionization of the LNP and negative correlation with number mean size but not with z-average size. As seen in SI Figure 5 those parameters unfortunately don't correlate with in vivo efficacy, which is reflected by low correlation between ratio and in vivo potency. Flow Rate, surprisingly, didn't correlate with physical parameters of the LNPs, although it had a slight positive correlation with in vivo efficacy (Figures 5A, 5B and 5C). The aqueous to ethanol solution ratio strongly correlated with LNP TNS fluorescence and entrapment while having a slight inverse correlation with LNP in vivo efficacy (Figures 5A, 5D and 5E). Also, no significant trends were seen when comparing flow rate and ratio with in vivo efficacy by organ (SI Figure 6).

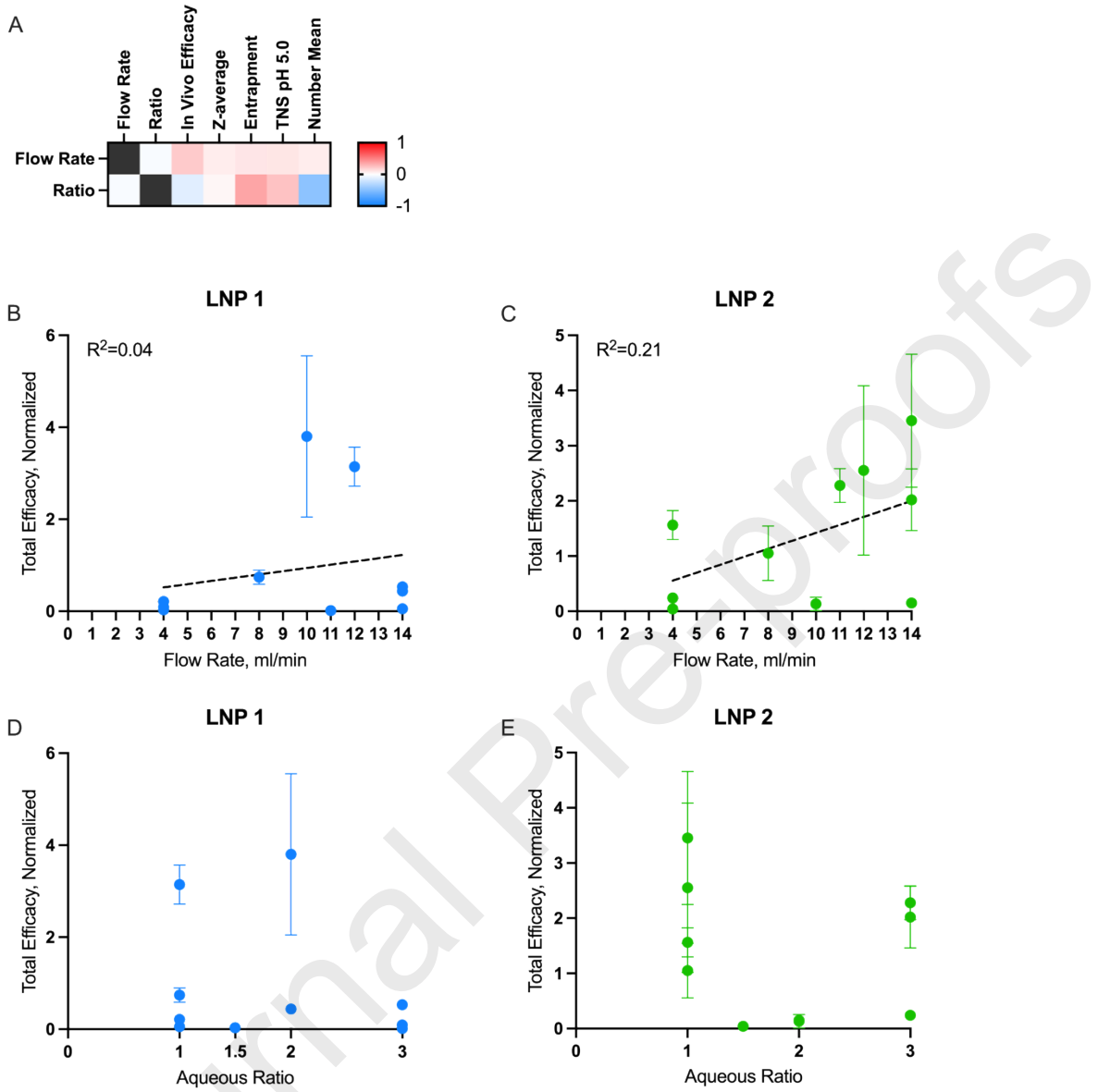

Figure 5. ***Microfluidic mixing parameters do not correlate well with efficacy or LNP physical characteristics.*** *A) Heatmap showing the correlations between microfluidic mixing conditions (total flow rate, aqueous : ethanol solutions ratio) and LNP physical characteristics. Correlation values of 1 and -1 represent perfect positive and inverse correlations, respectively. White indicates no correlation between the parameters. B) Total in vivo efficacy, normalized to manual formulation, of LNP 1 and C) LNP 2 vs. flow rate. D) Normalized total in vivo efficacy of LNP 1 and E) LNP 2 vs. the ratio of aqueous to ethanol solutions. n=3, error bars represent standard deviation.*

4. Discussion

In this study, we investigated the relationship between microfluidic mixing parameters and resulting LNP efficacy and organ tropism in comparison to LNPs mixed manually. We were motivated to examine this, in part, for anecdotal reasons: our own lab has struggled with the transition from manually mixed particles to those made via microfluidics, and there was limited literature guidance on overcoming this challenge. It was clear that a better understanding of this topic was needed.

This work demonstrates that the mixing methods used to generate LNPs affect their performance in mice in terms of mRNA delivery efficacy and organ tropism. Depending on the mixing parameters, LNP in vivo efficacy varied from 0.0025x to 4x the efficacy of the manually made LNP (Figure 2). Higher in vivo efficacy has been previously reported for flow rates of 10-20 ml/min and aqueous to ethanol ratios of 2:1 or 3:1 [40,46], which may occur due to smaller LNP size and higher uniformity of the particles [70]. Our data also show that LNPs made using microfluidic devices can perform up to 400 times worse that the manually made LNP.

Further, we found that mixing parameters differentially affected the performance of LNPs generated with distinct ionizable lipids (Figure 4). Even small changes in ionizable lipid structure led to differences in optimal mixing parameters: LNPs 1 and 3 contain a single carbon branch difference on their tails. This small alteration markedly affects LNP in vivo behavior but also, interestingly, their optimal mixing parameters. Further study is required to understand why such subtle chemical differences on one out of the five components in an LNP has such an impact on optimal mixing parameters. Based on these results, we anticipate that other alterations of the chemical formulation in terms of lipid ingredients, their molar ratios, and the weight ratio of lipid to mRNA will also impact mixing optimization.

We also found that mixing parameters influence the organ tropism of mRNA expression (Figure 3). Previous studies [71,72] have shown that increasing mol% of helper lipids and decreasing mol% of cholesterol in an LNP formulation can dramatically shift LNP organ tropism. It is possible that, despite identical mol% values in the lipid and RNA streams, that microfluidic and manual mixing generate LNPs that have incorporated varied mol% of ingredients. Our Z-average and number mean size data weakly correlated with efficiency or organ tropism, suggesting that there are additional factors altered by mixing methods that influence LNP.

It is also known that internal lipid packing influences LNP efficacy and tropism, and mixing parameters will affect the nanoprecipitation process and final packing. [73,74]. The influence on potency is likely driven by the critical role that lipid packing plays on the LNP's ability to escape the endosome [74,75]. Regarding tropism, we anticipate that lipid packing influences the surface composition of the LNPs and the resultant protein corona that forms in the bloodstream, which is known to affect organ distribution and expression [55,76,77]. In this case, we are unable to attribute altered tropism to differences in LNP size because our data show that LNPs of similar size also differ in their tropism in vivo.

New and potentially improved variations on microfluidic mixing have been consistently introduced over the last decade. Currently, there are several microfluidic chip architectures used for LNP manufacturing, including T-mixing, herringbone mixing, and, most recently, ring mixers [35,78,79]. While all three architectures differ in their fluid mechanics, they all include the parameter inputs of flow rate and solution ratios. Work has already begun to identify structural differences in LNPs made with different microfluidic mixing architectures [70]. More studies are needed to determine whether optimal mixing parameters are maintained across varied microfluidic platforms.

5. Conclusion

Here, we show that microfluidic mixing parameters significantly impact efficacy and organ tropism for LNPs known to be potent when mixed by hand. Depending on LNP chemistry and the mixing parameters used, LNP efficacy was either augmented or extinguished compared to those made manually. The nanoparticles with increased efficacy exhibited enhanced organ tropism in the liver. Although such an effect is desirable for liver therapy applications, mixing parameters will require more balanced optimization when extrahepatocellular targeting is desired. Overall, these data show that microfluidic mixing parameters will require optimization for each LNP chemistry and ultimate application.

Declaration of Competing Interest

Authors declare no financial or personal interest that could have influenced data or other work presented in this paper.

Acknowledgments

This research was funded by several grants and awards, including Defense Advanced Research Projects Agency (DARPA) grants number HR0011-19-2-0007 and D16AP00143 and National Institutes of Health (NIH) grant number DP2-HD098860. M.L.A. was supported by an NSF Graduate Research Fellowship Program award number DGE1745016. The NMR instrumentation at Carnegie Mellon University was partially supported by the NSF grants CHE-0130903, CHE-1039870 and CHE-1726525. Authors are grateful to R. Petersen for his feedback on the manuscript.

References:

[1] G. Chodick, L. Tene, R.S. Rotem, T. Patalon, S. Gazit, A. Ben-Tov, C. Weil, I. Goldshtein, G. Twig, D. Cohen, K. Muhsen, The effectiveness of the TWO-DOSE BNT162b2 vaccine: analysis of real-world data, Clin Infect Dis. 74 (2021) ciab438-. https://doi.org/10.1093/cid/ciab438.

[2] L.R. Baden, H.M.E. Sahly, B. Essink, K. Kotloff, S. Frey, R. Novak, D. Diemert, S.A. Spector, N. Rouphael, C.B. Creech, J. McGettigan, S. Khetan, N. Segall, J. Solis, A. Brosz, C. Fierro, H. Schwartz, K. Neuzil, L. Corey, P. Gilbert, H. Janes, D. Follmann, M. Marovich, J. Mascola, L. Polakowski, J. Ledgerwood, B.S. Graham, H. Bennett, R. Pajon, C. Knightly, B. Leav, W. Deng, H. Zhou, S. Han, M. Ivarsson, J. Miller, T. Zaks, C.S. Group, Efficacy and Safety of the mRNA-1273 SARS-CoV-2 Vaccine, New Engl J Med. 384 (2020) 403–416. https://doi.org/10.1056/nejmoa2035389.

[3] A. Conway, M. Mendel, K. Kim, K. McGovern, A. Boyko, L. Zhang, J.C. Miller, R.C. DeKelver, D.E. Paschon, B.L. Mui, P.J.C. Lin, Y.K. Tam, C. Barbosa, T. Redelmeier, M.C. Holmes, G. Lee, Non-viral Delivery of Zinc Finger Nuclease mRNA Enables Highly Efficient In Vivo Genome Editing of Multiple Therapeutic Gene Targets, Mol Ther. 27 (2019) 866–877. https://doi.org/10.1016/j.ymthe.2019.03.003.

[4] J.P. Han, M. Kim, B.S. Choi, J.H. Lee, G.S. Lee, M. Jeong, Y. Lee, E.-A. Kim, H.-K. Oh, N. Go, H. Lee, K.J. Lee, U.G. Kim, J.Y. Lee, S. Kim, J. Chang, H. Lee, D.W. Song, S.C. Yeom, In vivo delivery of CRISPR-Cas9 using lipid nanoparticles enables antithrombin gene editing for sustainable hemophilia A and B therapy, Sci Adv. 8 (2022) eabj6901. https://doi.org/10.1126/sciadv.abj6901.

[5] E. Kenjo, H. Hozumi, Y. Makita, K.A. Iwabuchi, N. Fujimoto, S. Matsumoto, M. Kimura, Y. Amano, M. Ifuku, Y. Naoe, N. Inukai, A. Hotta, Low immunogenicity of LNP allows repeated administrations of CRISPR-Cas9 mRNA into skeletal muscle in mice, Nat Commun. 12 (2021) 7101. https://doi.org/10.1038/s41467-021-26714-w.

[6] T. Jiang, J.M. Henderson, K. Coote, Y. Cheng, H.C. Valley, X.-O. Zhang, Q. Wang, L.H. Rhym, Y. Cao, G.A. Newby, H. Bihler, M. Mense, Z. Weng, D.G. Anderson, A.P. McCaffrey, D.R. Liu, W. Xue, Chemical modifications of adenine base editor mRNA and guide RNA expand its application scope, Nat Commun. 11 (2020) 1979. https://doi.org/10.1038/s41467-020-15892-8.

[7] J.D. Finn, A.R. Smith, M.C. Patel, L. Shaw, M.R. Youniss, J. van Heteren, T. Dirstine, C. Ciullo, R. Lescarbeau, J. Seitzer, R.R. Shah, A. Shah, D. Ling, J. Growe, M. Pink, E. Rohde, K.M. Wood, W.E. Salomon, W.F. Harrington, C. Dombrowski, W.R. Strapps, Y. Chang, D.V. Morrissey, A Single Administration of CRISPR/Cas9 Lipid Nanoparticles Achieves Robust and Persistent In Vivo Genome Editing, Cell Reports. 22 (2018) 2227–2235. https://doi.org/10.1016/j.celrep.2018.02.014.

[8] K. Musunuru, A.C. Chadwick, T. Mizoguchi, S.P. Garcia, J.E. DeNizio, C.W. Reiss, K. Wang, S. Iyer, C. Dutta, V. Clendaniel, M. Amaonye, A. Beach, K. Berth, S. Biswas, M.C. Braun, H.-M. Chen, T.V. Colace, J.D. Ganey, S.A. Gangopadhyay, R. Garrity, L.N. Kasiewicz, J. Lavoie, J.A. Madsen, Y. Matsumoto, A.M. Mazzola, Y.S. Nasrullah, J. Nneji, H. Ren, A. Sanjeev, M. Shay, M.R. Stahley, S.H.Y. Fan, Y.K. Tam, N.M. Gaudelli, G. Ciaramella, L.E. Stolz, P. Malyala, C.J.

Cheng, K.G. Rajeev, E. Rohde, A.M. Bellinger, S. Kathiresan, In vivo CRISPR base editing of PCSK9 durably lowers cholesterol in primates, Nature. 593 (2021) 429–434. https://doi.org/10.1038/s41586-021-03534-y.

[9] M. Qiu, Z. Glass, J. Chen, M. Haas, X. Jin, X. Zhao, X. Rui, Z. Ye, Y. Li, F. Zhang, Q. Xu, Lipid nanoparticle-mediated codelivery of Cas9 mRNA and single-guide RNA achieves liver-specific in vivo genome editing of Angptl3, Proc National Acad Sci. 118 (2021) e2020401118. https://doi.org/10.1073/pnas.2020401118.

[10] D. An, A. Frassetto, E. Jacquinet, M. Eybye, J. Milano, C. DeAntonis, V. Nguyen, R. Laureano, J. Milton, S. Sabnis, C.M. Lukacs, L.T. Guey, Long-term efficacy and safety of mRNA therapy in two murine models of methylmalonic acidemia, Ebiomedicine. 45 (2019) 519–528. https://doi.org/10.1016/j.ebiom.2019.07.003.

[11] D. An, J.L. Schneller, A. Frassetto, S. Liang, X. Zhu, J.-S. Park, M. Theisen, S.-J. Hong, J. Zhou, R. Rajendran, B. Levy, R. Howell, G. Besin, V. Presnyak, S. Sabnis, K.E. Murphy-Benenato, E.S. Kumarasinghe, T. Salerno, C. Mihai, C.M. Lukacs, R.J. Chandler, L.T. Guey, C.P. Venditti, P.G.V. Martini, Systemic Messenger RNA Therapy as a Treatment for Methylmalonic Acidemia, Cell Reports. 21 (2017) 3548–3558. https://doi.org/10.1016/j.celrep.2017.11.081.

[12] M.L. Cacicedo, C. Weinl-Tenbruck, D. Frank, M.J. Limeres, S. Wirsching, K. Hilbert, M.A.P. Famian, N. Horscroft, J.B. Hennermann, F. Zepp, F. Chevessier-Tünnesen, S. Gehring, Phenylalanine hydroxylase mRNA rescues the phenylketonuria phenotype in mice, Frontiers Bioeng Biotechnology. 10 (2022) 993298. https://doi.org/10.3389/fbioe.2022.993298.

[13] M. Qiu, Y. Tang, J. Chen, R. Muriph, Z. Ye, C. Huang, J. Evans, E.P. Henske, Q. Xu, Lung-selective mRNA delivery of synthetic lipid nanoparticles for the treatment of pulmonary lymphangioleiomyomatosis, Proc National Acad Sci. 119 (2022) e2116271119. https://doi.org/10.1073/pnas.2116271119.

[14] X. Yu, Z. Yang, Y. Zhang, J. Xia, J. Zhang, Q. Han, H. Yu, C. Wu, Y. Xu, W. Xu, W. Yang, Lipid Nanoparticle Delivery of Chemically Modified NGFR100W mRNA Alleviates Peripheral Neuropathy, Adv Healthc Mater. (2022) 2202127. https://doi.org/10.1002/adhm.202202127.

[15] L. Jiang, J.-S. Park, L. Yin, R. Laureano, E. Jacquinet, J. Yang, S. Liang, A. Frassetto, J. Zhuo, X. Yan, X. Zhu, S. Fortucci, K. Hoar, C. Mihai, C. Tunkey, V. Presnyak, K.E. Benenato, C.M. Lukacs, P.G.V. Martini, L.T. Guey, Dual mRNA therapy restores metabolic function in long-term studies in mice with propionic acidemia, Nat Commun. 11 (2020) 5339. https://doi.org/10.1038/s41467-020-19156-3.

[16] M. Mockey, E. Bourseau, V. Chandrashekhar, A. Chaudhuri, E. Lafosse, E.L. Cam, V.F.J. Quesniaux, B. Ryffel, C. Pichon, P. Midoux, mRNA-based cancer vaccine: prevention of B16 melanoma progression and metastasis by systemic injection of MART1 mRNA histidylated lipopolyplexes, Cancer Gene Therapy. 14 (2007) 802–814. https://doi.org/10.1038/sj.cgt.7701072.

[17] Y.-N. Fan, M. Li, Y.-L. Luo, Q. Chen, L. Wang, H.-B. Zhang, S. Shen, Z. Gu, J. Wang, Cationic lipid-assisted nanoparticles for delivery of mRNA cancer vaccine, Biomater Sci-Uk. 6 (2018) 3009–3018. https://doi.org/10.1039/c8bm00908b.

[18] M.A. Islam, Y. Xu, W. Tao, J.M. Ubellacker, M. Lim, D. Aum, G.Y. Lee, K. Zhou, H. Zope, M. Yu, W. Cao, J.T. Oswald, M. Dinarvand, M. Mahmoudi, R. Langer, P.W. Kantoff, O.C. Farokhzad, B.R. Zetter, J. Shi, Restoration of tumour-growth suppression in vivo via systemic nanoparticle-mediated delivery of PTEN mRNA, Nat Biomed Eng. 2 (2018) 850–864. https://doi.org/10.1038/s41551-018-0284-0.

[19] M.M. Billingsley, N. Singh, P. Ravikumar, R. Zhang, C.H. June, M.J. Mitchell, Ionizable Lipid Nanoparticle-Mediated mRNA Delivery for Human CAR T Cell Engineering, Nano Lett. 20 (2020) 1578–1589. https://doi.org/10.1021/acs.nanolett.9b04246.

[20] J. Chen, Z. Ye, C. Huang, M. Qiu, D. Song, Y. Li, Q. Xu, Lipid nanoparticle-mediated lymph node–targeting delivery of mRNA cancer vaccine elicits robust CD8+ T cell response, Proc National Acad Sci. 119 (2022) e2207841119. https://doi.org/10.1073/pnas.2207841119.

[21] O.S. Fenton, K.J. Kauffman, J.C. Kaczmarek, R.L. McClellan, S. Jhunjhunwala, M.W. Tibbitt, M.D. Zeng, E.A. Appel, J.R. Dorkin, F.F. Mir, J.H. Yang, M.A. Oberli, M.W. Heartlein, F. DeRosa, R. Langer, D.G. Anderson, Synthesis and Biological Evaluation of Ionizable Lipid Materials for the In Vivo Delivery of Messenger RNA to B Lymphocytes, Adv. Mater. 29 (2017) 1606944. https://doi.org/10.1002/adma.201606944.

[22] I. Lai, S. Swaminathan, V. Baylot, A. Mosley, R. Dhanasekaran, M. Gabay, D.W. Felsher, Lipid nanoparticles that deliver IL-12 messenger RNA suppress tumorigenesis in MYC oncogene-driven hepatocellular carcinoma, J Immunother Cancer. 6 (2018) 125. https://doi.org/10.1186/s40425-018-0431-x.

[23] S.H. Kiaie, N.M. Zolbanin, A. Ahmadi, R. Bagherifar, H. Valizadeh, F. Kashanchi, R. Jafari, Recent advances in mRNA-LNP therapeutics: immunological and pharmacological aspects, J Nanobiotechnol. 20 (2022) 276. https://doi.org/10.1186/s12951-022-01478-7.

[24] K.K.L. Phua, K.W. Leong, S.K. Nair, Transfection efficiency and transgene expression kinetics of mRNA delivered in naked and nanoparticle format, J Control Release. 166 (2013) 227–233. https://doi.org/10.1016/j.jconrel.2012.12.029.

[25] G. Tavernier, O. Andries, J. Demeester, N.N. Sanders, S.C.D. Smedt, J. Rejman, mRNA as gene therapeutic: How to control protein expression, J Control Release. 150 (2011) 238–247. https://doi.org/10.1016/j.jconrel.2010.10.020.

[26] J. Cao, M. Choi, E. Guadagnin, M. Soty, M. Silva, V. Verzieux, E. Weisser, A. Markel, J. Zhuo, S. Liang, L. Yin, A. Frassetto, A.-R. Graham, K. Burke, T. Ketova, C. Mihai, Z. Zalinger, B. Levy, G. Besin, M. Wolfrom, B. Tran, C. Tunkey, E. Owen, J. Sarkis, A. Dousis, V. Presnyak, C. Pepin, W. Zheng, L. Ci, M. Hard, E. Miracco, L. Rice, V. Nguyen, M. Zimmer, U. Rajarajacholan, P.F. Finn, G. Mithieux, F. Rajas, P.G.V. Martini, P.H. Giangrande, mRNA therapy restores euglycemia and prevents liver tumors in murine model of glycogen storage disease, Nat Commun. 12 (2021) 3090. https://doi.org/10.1038/s41467-021-23318-2.

[27] M. Inc, A Study of mRNA-3745 in Participants With Glycogen Storage Disease Type 1a (GSD1a), (2021). https://clinicaltrials.gov/ct2/show/study/NCT05095727 (accessed December 1, 2022).

[28] A.T. Inc., C. Schwabe, Safety, Tolerability and Pharmacokinetics of ARCT-810 in Healthy Adult Subjects, (2022). https://clinicaltrials.gov/ct2/show/NCT04416126 (accessed December 1, 2022).

[29] I. Therapeutics, Study to Evaluate Safety, Tolerability, Pharmacokinetics, and Pharmacodynamics of NTLA-2001 in Patients With Hereditary Transthyretin Amyloidosis With Polyneuropathy (ATTRv-PN) and Patients With Transthyretin Amyloidosis-Related Cardiomyopathy (ATTR-CM), (2020). https://clinicaltrials.gov/ct2/show/NCT04601051 (accessed December 1, 2022).

[30] J. Viger-Gravel, A. Schantz, A.C. Pinon, A.J. Rossini, S. Schantz, L. Emsley, Structure of Lipid Nanoparticles Containing siRNA or mRNA by Dynamic Nuclear Polarization-Enhanced NMR Spectroscopy, J Phys Chem B. 122 (2018) 2073–2081. https://doi.org/10.1021/acs.jpcb.7b10795.

[31] K.A. Hajj, K.A. Whitehead, Tools for translation: non-viral materials for therapeutic mRNA delivery, Nat Rev Mater. 2 (2017) 17056. https://doi.org/10.1038/natrevmats.2017.56.

[32] Y. Dong, W.K. Ng, S. Shen, S. Kim, R.B.H. Tan, Solid lipid nanoparticles: Continuous and potential large-scale nanoprecipitation production in static mixers, Colloids Surfaces B Biointerfaces. 94 (2012) 68–72. https://doi.org/10.1016/j.colsurfb.2012.01.018.

[33] N.M. Belliveau, J. Huft, P.J. Lin, S. Chen, A.K. Leung, T.J. Leaver, A.W. Wild, J.B. Lee, R.J. Taylor, Y.K. Tam, C.L. Hansen, P.R. Cullis, Microfluidic Synthesis of Highly Potent Limit-size Lipid Nanoparticles for In Vivo Delivery of siRNA, Mol Ther - Nucleic Acids. 1 (2012) e37. https://doi.org/10.1038/mtna.2012.28.

[34] R.C. Ryals, S. Patel, C. Acosta, M. McKinney, M.E. Pennesi, G. Sahay, The effects of PEGylation on LNP based mRNA delivery to the eye, Plos One. 15 (2020) e0241006. https://doi.org/10.1371/journal.pone.0241006.

[35] X. Wang, S. Liu, Y. Sun, X. Yu, S.M. Lee, Q. Cheng, T. Wei, J. Gong, J. Robinson, D. Zhang, X. Lian, P. Basak, D.J. Siegwart, Preparation of selective organ-targeting (SORT) lipid nanoparticles (LNPs) using multiple technical methods for tissue-specific mRNA delivery, Nat Protoc. (2022) 1–27. https://doi.org/10.1038/s41596-022-00755-x.

[36] S.C. Semple, A. Akinc, J. Chen, A.P. Sandhu, B.L. Mui, C.K. Cho, D.W.Y. Sah, D. Stebbing, E.J. Crosley, E. Yaworski, I.M. Hafez, J.R. Dorkin, J. Qin, K. Lam, K.G. Rajeev, K.F. Wong, L.B. Jeffs, L. Nechev, M.L. Eisenhardt, M. Jayaraman, M. Kazem, M.A. Maier, M. Srinivasulu, M.J. Weinstein, Q. Chen, R. Alvarez, S.A. Barros, S. De, S.K. Klimuk, T. Borland, V. Kosovrasti, W.L. Cantley, Y.K. Tam, M. Manoharan, M.A. Ciufolini, M.A. Tracy, A. de Fougerolles, I. MacLachlan, P.R. Cullis, T.D. Madden, M.J. Hope, Rational design of cationic lipids for siRNA delivery, Nat Biotechnol. 28 (2010) 172–176. https://doi.org/10.1038/nbt.1602.

[37] R.L. Ball, K.A. Hajj, J. Vizelman, P. Bajaj, K.A. Whitehead, Lipid Nanoparticle Formulations for Enhanced Co-delivery of siRNA and mRNA, Nano Lett. 18 (2018) 3814–3822. https://doi.org/10.1021/acs.nanolett.8b01101.

[38] K.T. Love, K.P. Mahon, C.G. Levins, K.A. Whitehead, W. Querbes, J.R. Dorkin, J. Qin, W. Cantley, L.L. Qin, T. Racie, M. Frank-Kamenetsky, K.N. Yip, R. Alvarez, D.W.Y. Sah, A. de

Fougerolles, K. Fitzgerald, V. Koteliansky, A. Akinc, R. Langer, D.G. Anderson, Lipid-like materials for low-dose, in vivo gene silencing, Proc National Acad Sci. 107 (2010) 1864–1869. https://doi.org/10.1073/pnas.0910603106.

[39] Y. Dong, K.T. Love, J.R. Dorkin, S. Sirirungruang, Y. Zhang, D. Chen, R.L. Bogorad, H. Yin, Y. Chen, A.J. Vegas, C.A. Alabi, G. Sahay, K.T. Olejnik, W. Wang, A. Schroeder, A.K.R. Lytton-Jean, D.J. Siegwart, A. Akinc, C. Barnes, S.A. Barros, M. Carioto, K. Fitzgerald, J. Hettinger, V. Kumar, T.I. Novobrantseva, J. Qin, W. Querbes, V. Koteliansky, R. Langer, D.G. Anderson, Lipopeptide nanoparticles for potent and selective siRNA delivery in rodents and nonhuman primates, Proc National Acad Sci. 111 (2014) 3955–3960. https://doi.org/10.1073/pnas.1322937111.

[40] K.J. Kauffman, J.R. Dorkin, J.H. Yang, M.W. Heartlein, F. DeRosa, F.F. Mir, O.S. Fenton, D.G. Anderson, Optimization of Lipid Nanoparticle Formulations for mRNA Delivery in Vivo with Fractional Factorial and Definitive Screening Designs, Nano Lett. 15 (2015) 7300–7306. https://doi.org/10.1021/acs.nanolett.5b02497.

[41] N. Kimura, M. Maeki, Y. Sato, Y. Note, A. Ishida, H. Tani, H. Harashima, M. Tokeshi, Development of the iLiNP Device: Fine Tuning the Lipid Nanoparticle Size within 10 nm for Drug Delivery, Acs Omega. 3 (2018) 5044–5051. https://doi.org/10.1021/acsomega.8b00341.

[42] K.J. Hassett, K.E. Benenato, E. Jacquinet, A. Lee, A. Woods, O. Yuzhakov, S. Himansu, J. Deterling, B.M. Geilich, T. Ketova, C. Mihai, A. Lynn, I. McFadyen, M.J. Moore, J.J. Senn, M.G. Stanton, Ö. Almarsson, G. Ciaramella, L.A. Brito, Optimization of Lipid Nanoparticles for Intramuscular Administration of mRNA Vaccines, Mol Ther Nucleic Acids. 15 (2019) 1–11. https://doi.org/10.1016/j.omtn.2019.01.013.

[43] M. Maeki, S. Uno, A. Niwa, Y. Okada, M. Tokeshi, Microfluidic technologies and devices for lipid nanoparticle-based RNA delivery, J Control Release. 344 (2022) 80–96. https://doi.org/10.1016/j.jconrel.2022.02.017.

[44] X. Wang, S. Liu, Y. Sun, X. Yu, S.M. Lee, Q. Cheng, T. Wei, J. Gong, J. Robinson, D. Zhang, X. Lian, P. Basak, D.J. Siegwart, Preparation of selective organ-targeting (SORT) lipid nanoparticles (LNPs) using multiple technical methods for tissue-specific mRNA delivery, Nat. Protoc. 18 (2023) 265–291. https://doi.org/10.1038/s41596-022-00755-x.

[45] N.M. Belliveau, J. Huft, P.J. Lin, S. Chen, A.K. Leung, T.J. Leaver, A.W. Wild, J.B. Lee, R.J. Taylor, Y.K. Tam, C.L. Hansen, P.R. Cullis, Microfluidic Synthesis of Highly Potent Limit-size Lipid Nanoparticles for In Vivo Delivery of siRNA, Mol Ther - Nucleic Acids. 1 (2012) e37. https://doi.org/10.1038/mtna.2012.28.

[46] D. Chen, K.T. Love, Y. Chen, A.A. Eltoukhy, C. Kastrup, G. Sahay, A. Jeon, Y. Dong, K.A. Whitehead, D.G. Anderson, Rapid Discovery of Potent siRNA-Containing Lipid Nanoparticles Enabled by Controlled Microfluidic Formulation, J Am Chem Soc. 134 (2012) 6948–6951. https://doi.org/10.1021/ja301621z.

[47] J. Ma, S.M.-Y. Lee, C. Yi, C.-W. Li, Controllable synthesis of functional nanoparticles by microfluidic platforms for biomedical applications – a review, Lab Chip. 17 (2016) 209–226. https://doi.org/10.1039/c6lc01049k.

[48] M.G.S. Correia, M.L. Briuglia, F. Niosi, D.A. Lamprou, Microfluidic manufacturing of phospholipid nanoparticles: Stability, encapsulation efficacy, and drug release, Int J Pharmaceut. 516 (2017) 91–99. https://doi.org/10.1016/j.ijpharm.2016.11.025.

[49] M.J.W. Evers, J.A. Kulkarni, R. der Meel, P.R. Cullis, P. Vader, R.M. Schiffelers, State-of-the-Art Design and Rapid-Mixing Production Techniques of Lipid Nanoparticles for Nucleic Acid Delivery, Small Methods. 2 (2018) 1700375. https://doi.org/10.1002/smtd.201700375.

[50] P.P.G. Guimaraes, R. Zhang, R. Spektor, M. Tan, A. Chung, M.M. Billingsley, R. El-Mayta, R.S. Riley, L. Wang, J.M. Wilson, M.J. Mitchell, Ionizable lipid nanoparticles encapsulating barcoded mRNA for accelerated in vivo delivery screening, J Control Release. 316 (2019) 404–417. https://doi.org/10.1016/j.jconrel.2019.10.028.

[51] J.B. Miller, S. Zhang, P. Kos, H. Xiong, K. Zhou, S.S. Perelman, H. Zhu, D.J. Siegwart, Non-Viral CRISPR/Cas Gene Editing In Vitro and In Vivo Enabled by Synthetic Nanoparticle Co-Delivery of Cas9 mRNA and sgRNA, Angew Chem-Ger Edit. 129 (2017) 1079–1083. https://doi.org/10.1002/ange.201610209.

[52] J.R. Hoffman, E. Tasciotti, R. Molinaro, Multiple Myeloma, Methods and Protocols, Methods Mol Biology. 1792 (2018) 205–214. https://doi.org/10.1007/978-1-4939-7865-6_15.

[53] K.A. Hajj, J.R. Melamed, N. Chaudhary, N.G. Lamson, R.L. Ball, S.S. Yerneni, K.A. Whitehead, A Potent Branched-Tail Lipid Nanoparticle Enables Multiplexed mRNA Delivery and Gene Editing In Vivo, Nano Lett. 20 (2020) 5167–5175. https://doi.org/10.1021/acs.nanolett.0c00596.

[54] D. Loughrey, J.E. Dahlman, Non-liver mRNA Delivery, Accounts Chem Res. 55 (2022) 13–23. https://doi.org/10.1021/acs.accounts.1c00601.

[55] M. Qiu, Y. Tang, J. Chen, R. Muriph, Z. Ye, C. Huang, J. Evans, E.P. Henske, Q. Xu, Lung-selective mRNA delivery of synthetic lipid nanoparticles for the treatment of pulmonary lymphangioleiomyomatosis, Proc National Acad Sci. 119 (2022) e2116271119. https://doi.org/10.1073/pnas.2116271119.

[56] C.D. Sago, M.P. Lokugamage, K. Paunovska, D.A. Vanover, C.M. Monaco, N.N. Shah, M.G. Castro, S.E. Anderson, T.G. Rudoltz, G.N. Lando, P.M. Tiwari, J.L. Kirschman, N. Willett, Y.C. Jang, P.J. Santangelo, A.V. Bryksin, J.E. Dahlman, High-throughput in vivo screen of functional mRNA delivery identifies nanoparticles for endothelial cell gene editing, P Natl Acad Sci Usa. 115 (2018) E9944–E9952. https://doi.org/10.1073/pnas.1811276115.

[57] M. Maeki, N. Kimura, Y. Sato, H. Harashima, M. Tokeshi, Advances in microfluidics for lipid nanoparticles and extracellular vesicles and applications in drug delivery systems, Adv Drug Deliver Rev. 128 (2018) 84–100. https://doi.org/10.1016/j.addr.2018.03.008.

[58] R.L. Ball, P. Bajaj, K.A. Whitehead, Achieving long-term stability of lipid nanoparticles: examining the effect of pH, temperature, and lyophilization, Int J Nanomed. 12 (2016) 305–315. https://doi.org/10.2147/ijn.s123062.

[59] K.A. Hajj, R.L. Ball, S.B. Deluty, S.R. Singh, D. Strelkova, C.M. Knapp, K.A. Whitehead, Branched-Tail Lipid Nanoparticles Potently Deliver mRNA In Vivo due to Enhanced Ionization at Endosomal pH, Small. 15 (2019) 1805097. https://doi.org/10.1002/smll.201805097.

[60] X. Huang, X. Zhao, L. Wang, M. Zhao, P. Xie, D. Yang, 17 Delivery of betulinic acid lipid nanoparticles assembled by a microfluidic device, J Invest Med. 64 (2016) A6. https://doi.org/10.1136/jim-2016-000328.17.

[61] N. Kimura, M. Maeki, Y. Sato, Y. Note, A. Ishida, H. Tani, H. Harashima, M. Tokeshi, Development of the iLiNP Device: Fine Tuning the Lipid Nanoparticle Size within 10 nm for Drug Delivery, Acs Omega. 3 (2018) 5044–5051. https://doi.org/10.1021/acsomega.8b00341.

[62] J.A. Kulkarni, M.M. Darjuan, J.E. Mercer, S. Chen, R. van der Meel, J.L. Thewalt, Y.Y.C. Tam, P.R. Cullis, On the Formation and Morphology of Lipid Nanoparticles Containing Ionizable Cationic Lipids and siRNA, Acs Nano. 12 (2018) 4787–4795. https://doi.org/10.1021/acsnano.8b01516.

[63] C.B. Roces, G. Lou, N. Jain, S. Abraham, A. Thomas, G.W. Halbert, Y. Perrie, Manufacturing Considerations for the Development of Lipid Nanoparticles Using Microfluidics, Pharm. 12 (2020) 1095. https://doi.org/10.3390/pharmaceutics12111095.

[64] A.K.K. Leung, Y.Y.C. Tam, S. Chen, I.M. Hafez, P.R. Cullis, Microfluidic Mixing: A General Method for Encapsulating Macromolecules in Lipid Nanoparticle Systems, J Phys Chem B. 119 (2015) 8698–8706. https://doi.org/10.1021/acs.jpcb.5b02891.

[65] J.R. Melamed, K.A. Hajj, N. Chaudhary, D. Strelkova, M.L. Arral, N. Pardi, M.-G. Alameh, J.B. Miller, L. Farbiak, D.J. Siegwart, D. Weissman, K.A. Whitehead, Lipid nanoparticle chemistry determines how nucleoside base modifications alter mRNA delivery, J Control Release. 341 (2022) 206–214. https://doi.org/10.1016/j.jconrel.2021.11.022.

[66] K.J. Kauffman, J.R. Dorkin, J.H. Yang, M.W. Heartlein, F. DeRosa, F.F. Mir, O.S. Fenton, D.G. Anderson, Optimization of Lipid Nanoparticle Formulations for mRNA Delivery in Vivo with Fractional Factorial and Definitive Screening Designs, Nano Lett. 15 (2015) 7300–7306. https://doi.org/10.1021/acs.nanolett.5b02497.

[67] M.A. Oberli, A.M. Reichmuth, J.R. Dorkin, M.J. Mitchell, O.S. Fenton, A. Jaklenec, D.G. Anderson, R. Langer, D. Blankschtein, Lipid Nanoparticle Assisted mRNA Delivery for Potent Cancer Immunotherapy, Nano Lett. 17 (2016) 1326–1335. https://doi.org/10.1021/acs.nanolett.6b03329.

[68] K.A. Whitehead, J. Matthews, P.H. Chang, F. Niroui, J.R. Dorkin, M. Severgnini, D.G. Anderson, In Vitro–In Vivo Translation of Lipid Nanoparticles for Hepatocellular siRNA Delivery, Acs Nano. 6 (2012) 6922–6929. https://doi.org/10.1021/nn301922x.

[69] M.M. Billingsley, N. Singh, P. Ravikumar, R. Zhang, C.H. June, M.J. Mitchell, Ionizable Lipid Nanoparticle-Mediated mRNA Delivery for Human CAR T Cell Engineering, Nano Lett. 20 (2020) 1578–1589. https://doi.org/10.1021/acs.nanolett.9b04246.

[70] C.B. Roces, G. Lou, N. Jain, S. Abraham, A. Thomas, G.W. Halbert, Y. Perrie, Manufacturing Considerations for the Development of Lipid Nanoparticles Using Microfluidics, Pharm. 12 (2020) 1095. https://doi.org/10.3390/pharmaceutics12111095.

[71] S.T. LoPresti, M.L. Arral, N. Chaudhary, K.A. Whitehead, The replacement of helper lipids with charged alternatives in lipid nanoparticles facilitates targeted mRNA delivery to the spleen and lungs, J Control Release. 345 (2022) 819–831. https://doi.org/10.1016/j.jconrel.2022.03.046.

[72] Q. Cheng, T. Wei, L. Farbiak, L.T. Johnson, S.A. Dilliard, D.J. Siegwart, Selective organ targeting (SORT) nanoparticles for tissue-specific mRNA delivery and CRISPR–Cas gene editing, Nat Nanotechnol. 15 (2020) 313–320. https://doi.org/10.1038/s41565-020-0669-6.

[73] P. Zhao, X. Hou, J. Yan, S. Du, Y. Xue, W. Li, G. Xiang, Y. Dong, Long-term storage of lipid-like nanoparticles for mRNA delivery, Bioact Mater. 5 (2020) 358–363. https://doi.org/10.1016/j.bioactmat.2020.03.001.

[74] M.E. Gindy, K. DiFelice, V. Kumar, R.K. Prud'homme, R. Celano, R.M. Haas, J.S. Smith, D. Boardman, Mechanism of Macromolecular Structure Evolution in Self-Assembled Lipid Nanoparticles for siRNA Delivery, Langmuir. 30 (2014) 4613–4622. https://doi.org/10.1021/la500630h.

[75] Y. Sato, Y. Note, M. Maeki, N. Kaji, Y. Baba, M. Tokeshi, H. Harashima, Elucidation of the physicochemical properties and potency of siRNA-loaded small-sized lipid nanoparticles for siRNA delivery, J Control Release. 229 (2016) 48–57. https://doi.org/10.1016/j.jconrel.2016.03.019.

[76] G. Caracciolo, D. Pozzi, A.L. Capriotti, C. Cavaliere, P. Foglia, H. Amenitsch, A. Laganà, Evolution of the Protein Corona of Lipid Gene Vectors as a Function of Plasma Concentration, Langmuir. 27 (2011) 15048–15053. https://doi.org/10.1021/la202912f.

[77] G. Caracciolo, D. Pozzi, S.C.D. Sanctis, A.L. Capriotti, G. Caruso, R. Samperi, A. Laganà, Effect of membrane charge density on the protein corona of cationic liposomes: Interplay between cationic charge and surface area, Appl Phys Lett. 99 (2011) 033702. https://doi.org/10.1063/1.3615055.

[78] M. Ripoll, E. Martin, M. Enot, O. Robbe, C. Rapisarda, M.-C. Nicolai, A. Deliot, P. Tabeling, J.-R. Authelin, M. Nakach, P. Wils, Optimal self-assembly of lipid nanoparticles (LNP) in a ring micromixer, Sci Rep-Uk. 12 (2022) 9483. https://doi.org/10.1038/s41598-022-13112-5.

[79] C. Webb, N. Forbes, C.B. Roces, G. Anderluzzi, G. Lou, S. Abraham, L. Ingalls, K. Marshall, T.J. Leaver, J.A. Watts, J.W. Aylott, Y. Perrie, Using microfluidics for scalable manufacturing of nanomedicines from bench to GMP: A case study using protein-loaded liposomes, Int J Pharmaceut. 582 (2020) 119266. https://doi.org/10.1016/j.ijpharm.2020.119266.

Supplementary Information:

Materials and Methods

503 and 514 Amine Heads Synthesis

In a 250 mL round bottom flask, sodium meta-bisulfite (1.065 equiv) was dissolved in deionized water (67 mL) with stirring. Then, 37% aqueous formaldehyde (2 equiv, Sigma Aldrich) was added to the mixture by a syringe and refluxed for 10 min. Once cooled to room temperature, N,N′-diethyl-1,3-propanediamine (1 equiv., TCI, 514 Starting material) was added with vigorous stirring for 4 h. Sodium cyanide (2.25 equiv, Alfa Aesar) was dissolved in deionized water (33 mL), added to the reaction mixture, and stirred o/n (CAUTION: NaCN is EXTREMELY TOXIC, handle with the utmost care). The reaction mixture was transferred to a separatory funnel with saturated NaCl (175 mL). The aqueous layer was extracted 3 times with dichloromethane (150 mL). The combined organic layers were dried over magnesium sulfate, filtered, and concentrated via rotary evaporation. The concentrate was purified by chromatography using basic alumina and dichloromethane as the eluent. The product was 514-CN. This process was repeated with N^1,N^3-dimethylpropane-1,3-diamine (TCI, 503 starting material), and the product was 503-CN.

All glassware was dried overnight in a 140°C oven. A 1000 mL 3-neck round bottom flask with a condenser, glass stopper, gas adapter, and an unpierced septum was assembled under nitrogen gas. The reaction vessel was cycled under vacuum and nitrogen gas three times and then charged with dry inhibitor-free tetrahydrofuran (200 mL, Sigma Aldrich). On an ice bath, lithium aluminum hydride (4.6 equiv, Sigma Aldrich) was added to the tetrahydrofuran in portions to create a suspension. A 500 mL Schlenk flask was cycled under vacuum and nitrogen gas three times and 514-CN (1 equiv) was added to the flask. Tetrahydrofuran (200 mL) was added to the Schlenk flask to dissolve the 514-CN. The solution of 514-CN was then added to the reaction vessel slowly. Then the vessel was allowed to reflux for 4 h. Once cooled to room temperature, diethyl ether (150 mL) was added. Then the reaction vessel was placed in an ice bath. To quench the reaction, water (4.2 mL), 15% aqueous NaOH (4.2 mL), and water (12.6 mL) was added dropwise to the reaction mixture in succession (CAUTION: Extremely REACTIVE, add water slowly). The ice bath was removed, the vessel brought to room temperature, and allowed to stir for 15 minutes. The product was then dried via magnesium sulfate, filtered, and concentrated via rotary evaporation. The concentrate was purified by chromatography over silica using dichloromethane/methanol/ammonium hydroxide (60/30/10) as the eluent. Product was confirmed with ^{1}H NMR spectroscopy. Final products were head groups 514 and 503.

$O_{6,10}$ acrylate tail

This tail was synthesized by reacting alcohol (2-Hexyl-1-Decanol, Sigma Aldrich) with acryloyl chloride (Alfa Aesar) and trimethylamine (Sigma Aldrich) at a molar ratio of 1:1.5:2 in reagent grade acetone (Spectrum) in a round bottom flask on ice. Ice was removed after ten minutes. Flask was allowed to equilibrate to room temperature and react for two hours. Quenching of the reaction was done with 3 mL of deionized water for ten minutes. Product was then rotary evaporated for ~ 1.5 hours, dissolved in ethyl acetate, and placed in a separation funnel. Four washes were performed to remove contaminants: 1) NaCl (saturated) and water in 1:1 volume ratio, 2) 1 N HCl and water in 1:1 volume ratio, 3) $NaHCO_3$ (saturated), and 4) NaCl (saturated). Once the product dissolved in ethyl acetate was separated, 3-6 mg of 2,5 Di-tert-butylhydroquinone was added to prevent polymerization. The product solution was dried over magnesium sulfate and removed by filtration. The product was isolated by rotary evaporation. Tail purification was performed using Teledyne ISCO Chromatography with dichloromethane as the mobile phase and silica gel as the stationary phase. The structure of the $O_{6,10}$ tail product was confirmed by ^{1}H (500 MHz) and ^{13}C (125 MHz) NMR spectroscopy on a Bruker spectrometer.

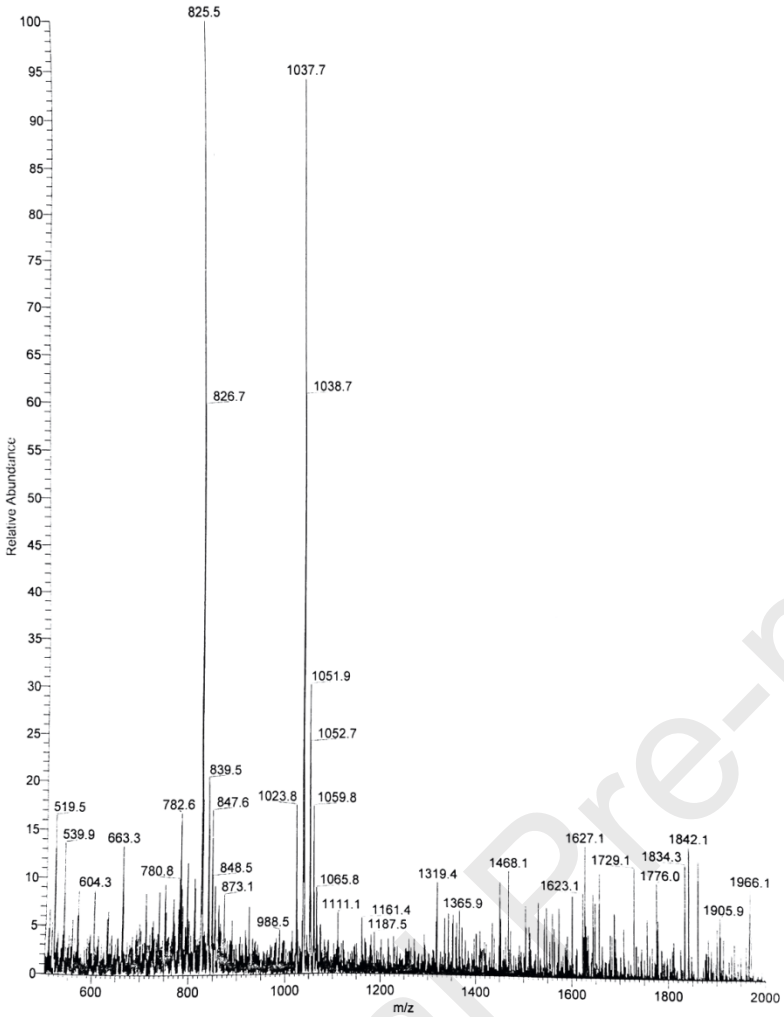

SI Figure 1. Mass spectrum of the $503O_{i10}$ lipidoid.

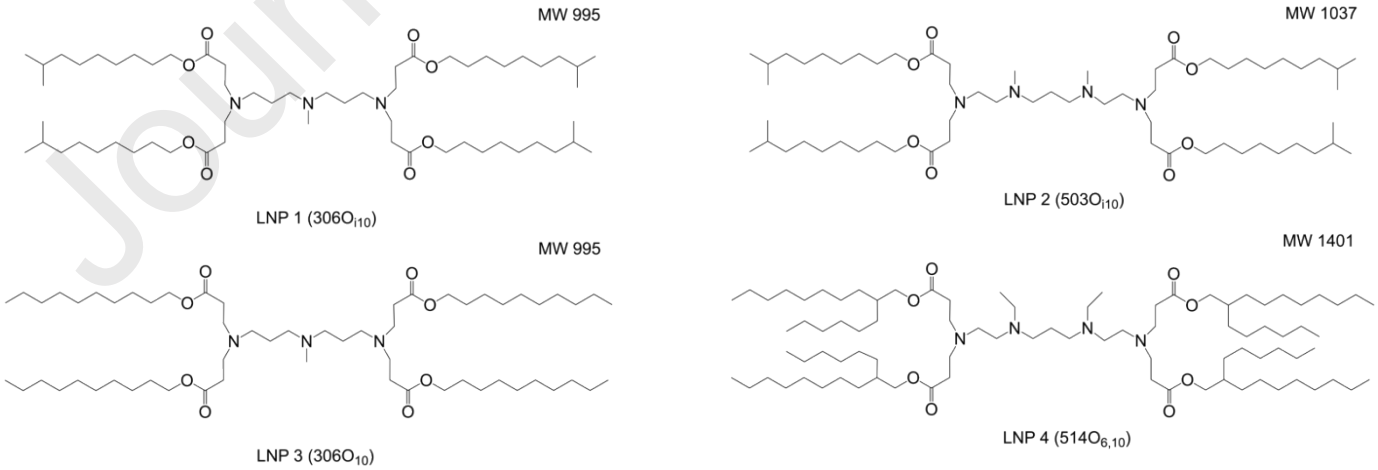

SI Figure 2. The four ionizable lipidoids used in the study. MW indicates molecular weight in g/mol.

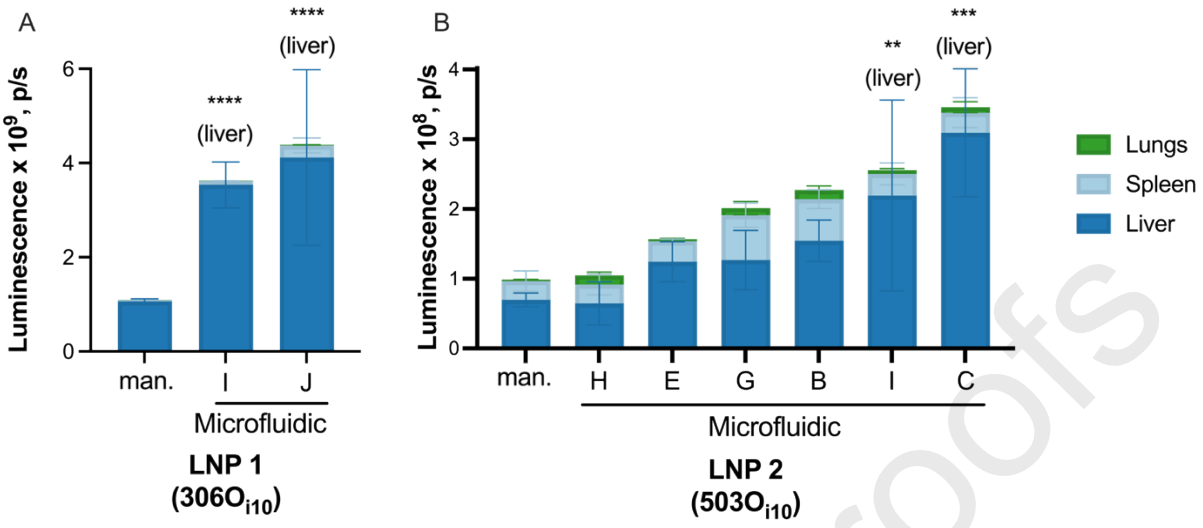

Figure 3. Improved efficacy of LNPs generated using microfluidics vs manual is due to improved delivery to the liver and, sometimes, spleen. Microfluidic LNPs with >25% of the manually mixed (man.) LNPs efficacy are shown here. LNPs were formulated with mRNA encoding firefly luciferase and delivered to mice at a total mRNA dose of 0.5 mg/kg. A) When generated using microfluidic mixing conditions I and J, LNP 1 had significantly higher signal in the liver compared to the manual formulation and increased spleen signal for condition J. B) When generated with a microfluidic device, LNP 2 showed increased signal in the liver compared to the manual formulation. N = 3, error bars represent standard deviation, **, ***, **** indicate p<0.01, p<0.001 and p<0.0001 respectively, for liver efficacy, according to a Tukey multiple comparison analysis after two-way ANOVA.

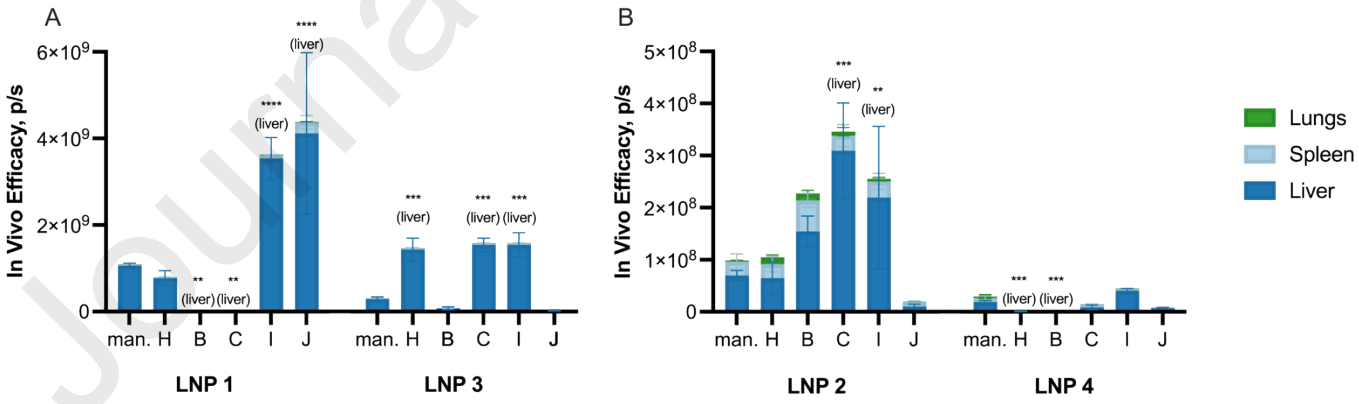

SI Figure 4. The most effective mixing conditions were inconsistent across LNP formulations. LNPs 1-4 were generated using five sets of mixing conditions. Mice were IV-injected with mRNA encoding firefly luciferase at a total dose of 0.5 mg/kg and imaged using IVIS three hours post-injection. Luciferase expression for A) LNPs 1 and 3 and B) LNPs 2 and 4 are shown by organ. N = 3, error bars represent standard deviation. **, ***, **** represent p<0.01, 0.001 and 0.0001, respectively, for liver signal, compared to the efficacy of manually formulated LNPs according to two-way ANOVA followed up by Dunnett multiple comparison.

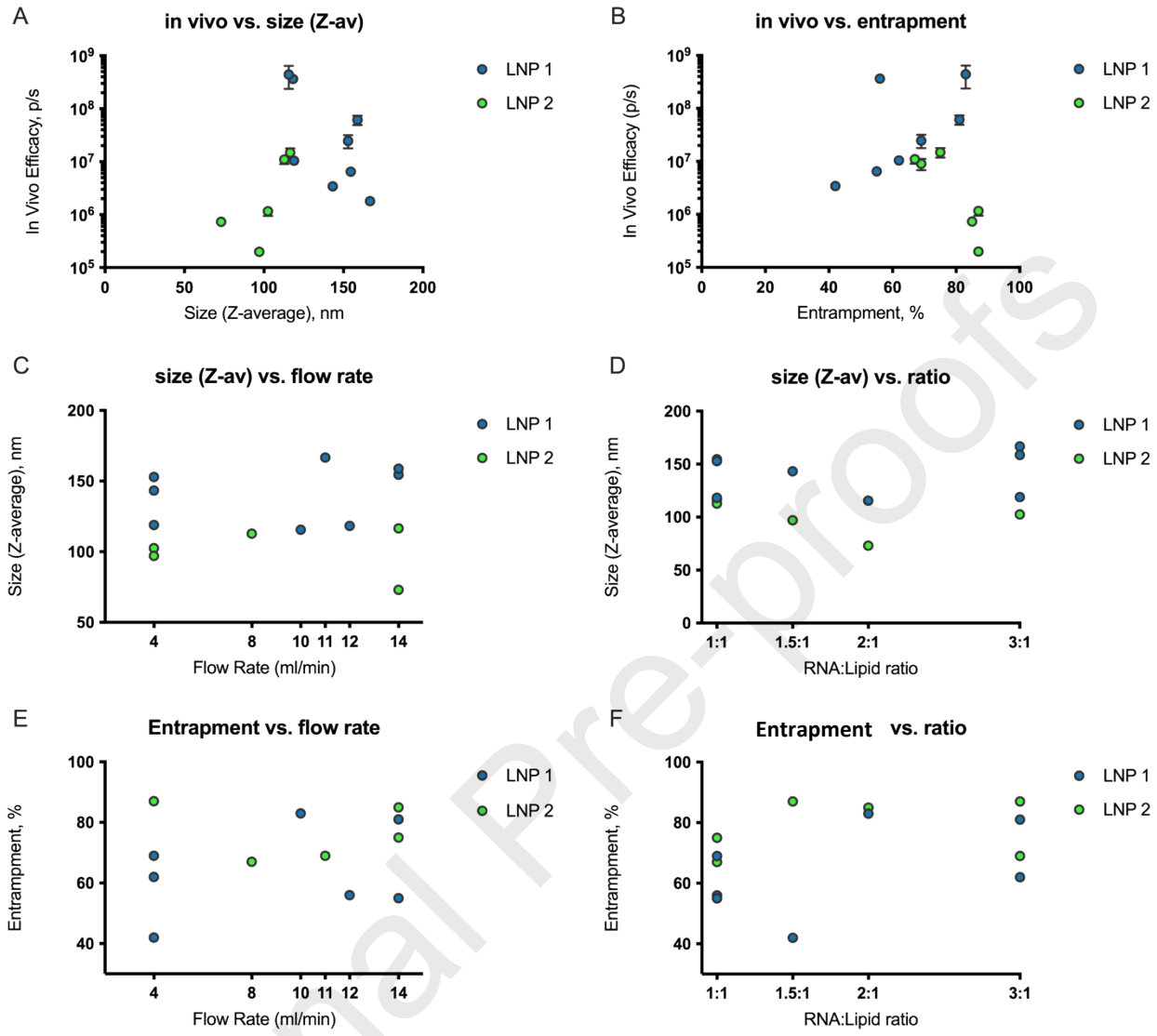

G

	LNP	N-mean, nm	Z-average, nm	PDI	Entrapment, %	TNS 5 fluorescence, au
$306O_{i10}$	1	80.0	114.7	0.100	86	32563
$503O_{i10}$	2	54.2	80.9	0.113	76	10698
$306O_{10}$	3	82.3	116.0	0.107	94	26505
$514O_{6,10}$	4	102.3	143.6	0.114	79	16081

SI Figure 5. There are no correlations between mixing parameters, LNP characterization results, or in vivo efficacy. LNPs made with microfluidic mixing were measured for size and entrapment. Resultant data were correlated with in vivo potency (A, B), flow rate (C, E) or mRNA to lipid ratio (D, F). G shows size (N-mean, Z-average, and PDI), entrapment, and TNS ionization at pH 5 (TNS 5) data for manually mixed LNPs 1-4. N = 3. Error bars represent standard deviation and are not shown for C-F for ease of reading the graph.

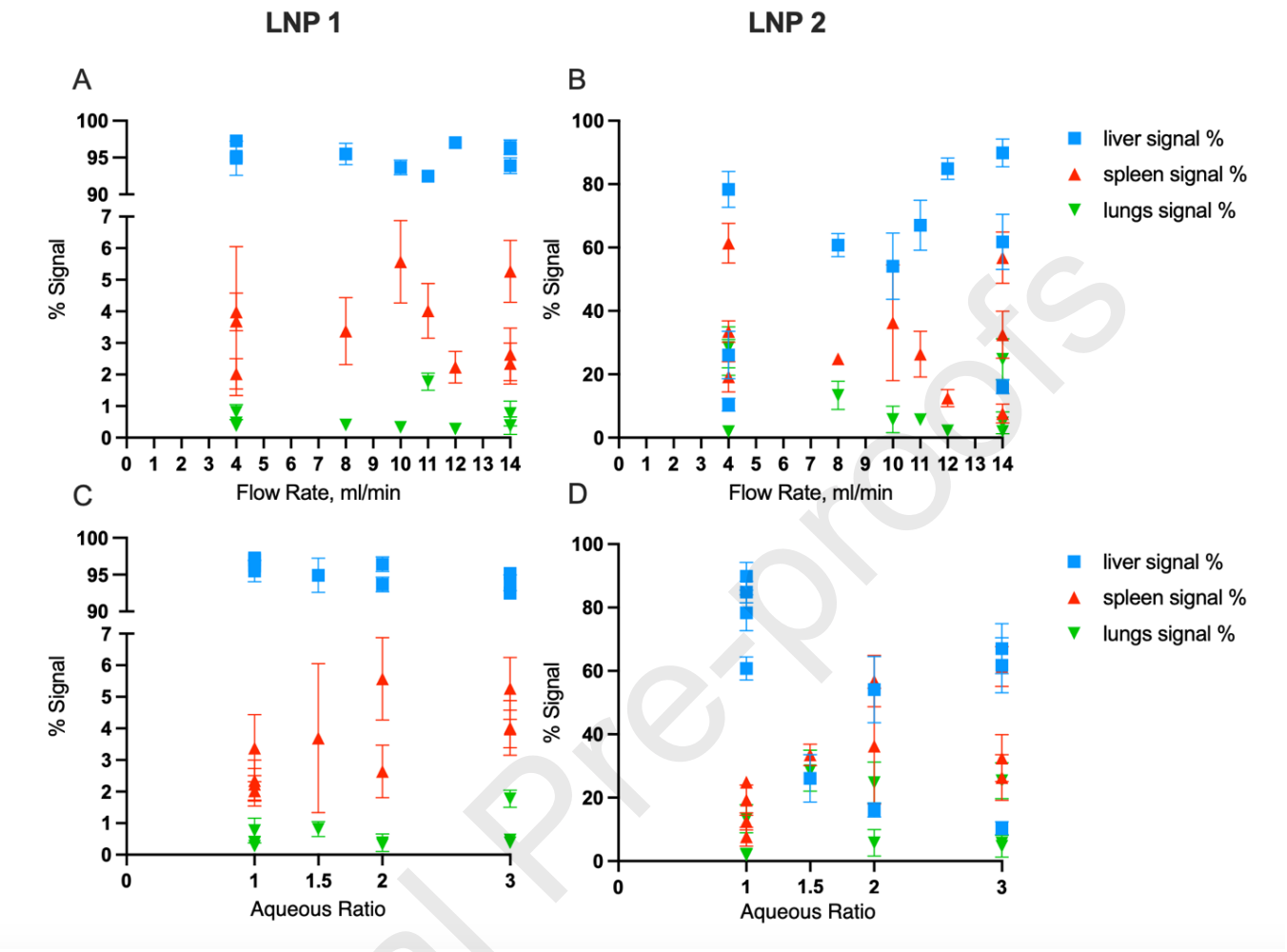

SI Figure 6. Mixing parameters did not correlate with efficacy distribution to the liver, spleen, or lungs. Graphs show efficacy organ distribution as a function of A, B) flow rate and C, D) aqueous to ethanol ratio. N = 3, error bars represent standard deviation.